Benha University

Faculty of Engineering at Shoubra

Mechanical Engineering Department

"Performance Study and Analysis of a Concentrated Solar Still"

A thesis submitted to the Faculty of Engineering at Shoubra, Benha University in partial fulfillment of the requirements for the degree of Master of Science in Mechanical Engineering (Mechanical Power Engineering)

Submitted by

Eng. Mohammad Mahmoud Daif Mohammad

B.Sc. in Mechanical Power Engineering
Faculty of Engineering at Shoubra–Benha University

Under the supervision of

Prof. Dr. Ahmed Attia Abdellatif

Mechanical Engineering Department
Faculty of Engineering at Shoubra
Benha University

Assoc. Prof. Dr. Mohamed Elsayed Mohamed Emam

Mechanical Engineering Department
Faculty of Engineering at Shoubra
Benha University

Dr. Aly Mohamed Ahmed Soliman

Mechanical Engineering Department
Faculty of Engineering at Shoubra
Benha University

Cairo − Egypt
2024

ACKNOWLEDGMENT

First and foremost, I express my deepest gratitude to Allah, the Almighty, for His blessings, and grace throughout this journey, and has granted us success to complete this research project.

I want to extend my heartfelt appreciation to Prof. Dr. **Ahmed Attia**, whose invaluable mentorship, expertise, and encouragement have been instrumental in shaping my academic journey. His dedication to excellence and commitment to scholarly pursuits have inspired me every step of the way.

I am also immensely grateful to my supervisors, Assoc. Prof. Dr. **Mohamed Emam** and Dr. **Aly Soliman**, for their guidance, support, and invaluable feedback throughout this research endeavor that has played a key role in navigating the complexities of this project.

Furthermore, I extend my sincere thanks to Assoc. Prof. Dr. **Mohamed Abdelrahman**, whose insightful advice, constructive criticism, and invaluable contributions have enriched this research and broadened my perspective.

Last but not least, I would like to thank my colleague Eng. **Mohamed Nasser** for his collaboration, support, and camaraderie throughout this journey. His dedication and friendship have been a source of inspiration and motivation.

To my dear family, whose unconditional love, unwavering support, and sacrifices have been the cornerstone of my success, I am eternally grateful. Your encouragement, understanding, and belief in my abilities have sustained me through the challenges and triumphs of this journey. This achievement is as much yours as it is mine, and I dedicate it to you with profound gratitude and love.

ABSTRACT

Water scarcity remains a critical global challenge, particularly in arid and semi-arid regions where access to freshwater is limited. In such contexts, the development of efficient and sustainable methods for freshwater production is of paramount importance to ensure the well-being of communities and the preservation of ecosystems. Concentrated solar stills offer a promising avenue for addressing this challenge by harnessing solar energy to produce distilled water from saline or brackish water sources.

The present study experimentally assessed a novel sun-tracking concentrated solar still within Egyptian climatic conditions during the summer of 2022. The proposed solar still system comprises a 1.2 m diameter parabolic reflector mirror equipped with a dual-axis tracking mechanism, ensuring optimal solar energy capture throughout the day. Coupled with a cylindrical solar still featuring a volume of 0.0037 m^3 positioned at the focal point, the system has a concentration ratio of 12.5, maximizing the efficiency of water vaporization and condensation processes.

Two important parameters are explored in this investigation: the salinity of the feed water and the filling ratio of saline water within the solar still. By evaluating three samples of feed water with varying salinity levels (17, 27, and 37 ppt) and four different filling ratios of saline water (26.5%, 39.8%, 53.1%, and 66.3%), insights into the impact of these factors on the system's performance are sought.

While augmenting the salinity of the feed water exhibited negligible impact on solar still productivity, variations in the saline water filling ratio yielded noticeable effects. The study indicated that elevating the filling ratio from 26.5% to 53.1% led to notable enhancement in both daily cumulative productivity and system efficiency by 22.69% and 26.34%, respectively. However, a further increase in the

filling ratio to 66.3% resulted in decreased daily cumulative productivity and system efficiency by 7.06% and 6.87%, respectively. Additionally, augmenting the feed water salinity from 17 ppt to 37 ppt led to a reduction in daily cumulative productivity by approximately 5.61% and daily system efficiency by 5.1%.

The daily cumulative productivity of the system was determined to be 6 kg/m^2, for an optimal filling ratio of 53.1%, achieving a daily efficiency rate of 42.88%. Additionally, the average cost associated with freshwater production was estimated at 0.0489 $/kg. Notably, the proposed system attained the highest instantaneous efficiency of 61.77% and the maximum distilled water productivity rate of 0.941 $kg/hr.m^2$.

CONTENTS

LIST OF FIGURES

LIST OF TABLES

NOMENCLATURE

Symbol	Description	Unit
A	Area	m^2
CR	Concentration ratio	-
DNI	Direct normal irradiance	W/m^2
f_s	Shading factor	-
h	Convection heat transfer coefficient	$W/m^2.K$
h_{fg}	Water latent heat of vaporization	J/kg
k	Thermal conductivity	W/m.K
L_c	Characteristic length	m
$m_{distilled}$	Mass of distilled yield	kg
Nu	Nusselt number	-
Q	Heat transfer rate	W
Re	Reynolds number	-
T	Temperature	K
V_{wind}	Velocity of wind	m/s

GREEK LETTERS

Symbol	Description	Unit
Δt	Time interval	s
ε	Emissivity	-
η	Efficiency	%
θ	The angle formed by the absorber plate and the vertical	°
ν	Kinematic viscosity	m^2/s
ρ	Reflectivity	-
σ	Stefan-Boltzmann constant	$W/m^2.K^4$
Φ	Filling ratio	%
ω	Uncertainty	-
Γ	Intercept factor	-

SUBSCRIPTS

Symbol	Description
abs	Absorber
amb	Ambient air
conc	Concentrated
conv	Convection
emit	Emitted
ref	Reflected
sys	System

ABBREVIATION

CPL	Cost Per Liter
CSS	Conventional Solar Still
ED	Electro-Dialysis
FO	Forward Osmosis
HDH	Humidification Dehumidification
HP	Horsepower
IX	Ion Exchange
MED	Multi-Effect Distillation
MSF	Multi-Stage Flash
MVC	Mechanical Vapor Compression
OL	Over Limit
PCM	Phase Change Material
ppt	Part Per Thousand
PV	Photovoltaic
RO	Reverse Osmosis
SD	Secure Digital
SDC	Solar Dish Concentrator
SS	Solar Still
TDS	Total Dissolved Solids
TVC	Thermal Vapor Compression

CHAPTER 1

INTRODUCTION

1.1 Background

The increasing demand for a reliable, uncontaminated, and uninterrupted freshwater supply has prompted extensive research and inquiries into water desalination and treatment methodologies. Despite the Earth's significant water coverage, with oceans and ice glaciers accounting for two-thirds of its surface, approximately 97% of this water is saline, leaving only a mere 3% as freshwater resources. Moreover, within the freshwater category, a substantial portion about 79% is locked within ice caps and glaciers, while groundwater sources constitute 29%. Consequently, only a scant 1% of freshwater reserves are readily accessible for consumption and utilization [1].

Water is a fundamental and indispensable resource vital for sustenance and development, serving essential purposes such as drinking, sanitation, agricultural irrigation, and industrial operations. However, the existing freshwater reservoirs are insufficient to meet the escalating demands of the expanding global population. Moreover, human activities have significantly contaminated many freshwater sources, exacerbating the scarcity issue. Consequently, there is an escalating necessity for water desalination technologies to bridge the gap between demand and supply. Additionally, the lack of accessible freshwater in rural areas poses a challenging obstacle to habitation and development in these regions.

Egypt heavily depends on the Nile River as its main source of freshwater, both in terms of quantity and quality. However, the sustainability of this vital resource is at risk due to the discharge of industrial waste into its water. The increasing demand for freshwater, both to offset potential losses from the Nile and to provide for remote

regions not directly served by the river, has underscored the urgent necessity for water desalination technologies in the country.

1.2 Water Desalination Technologies

Water desalination is a process designed to remove minerals, salts, and impurities from saline water, thereby producing freshwater suitable for various human applications.

Desalination methods can be classified based on the separation mechanism employed, which typically falls into two categories: evaporation and condensation (distillation), and membrane desalination. This classification is depicted in Fig. 1.1.

In distillation-based desalination, the principle involves supplying energy to saline water to generate vapor, which is then condensed to yield freshwater, effectively separating it from the salt. Common technologies in this category include Multi-Stage Flash (MSF), Multi-Effect Distillation (MED), Humidification Dehumidification (HDH), Vapor Compression, either Thermal (TVC) or Mechanical (MVC), and Solar Still (SS).

On the other hand, membrane desalination relies on passing saline water through a semi-permeable membrane, which selectively allows water molecules to pass through while trapping salts and impurities behind. Major technologies in this category include Reverse Osmosis (RO), Forward Osmosis (FO), Electro-Dialysis (ED), and Ion Exchange (IX).

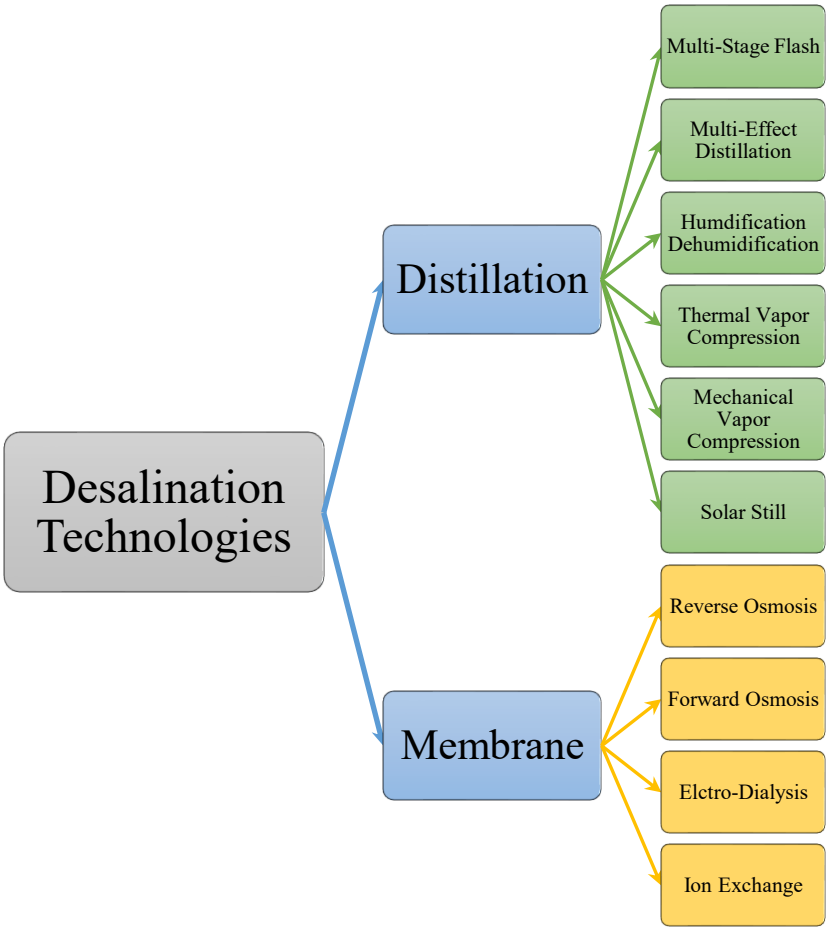

Fig. 1.1 Desalination technologies [2].

The desalination process demands a significant energy input and relying on fossil fuels as the primary energy source is no longer deemed optimal due to its adverse environmental effects, coupled with limitations and associated costs [3]. Thus, an alternative solution is imperative.

Renewable energy sources, characterized by their abundant availability and rapid replenishment rates, present a promising alternative [4]. Solar, wind, geothermal, hydropower, and bioenergy are among the various forms of renewable energy that can effectively replace fossil fuels in powering water desalination processes.

Egypt's location within the Earth's Sun Belt ensures abundant sunlight, with an average of 9-11 hours of sunlight per day. According to the solar atlas, daily direct normal irradiance (DNI) in Egypt ranges from 5.6 to 7.6 kWh/m^2 [5]. Furthermore, Egypt benefits from ample saline water sources from both the Mediterranean and Red Seas.

Given these factors, water desalination utilizing solar energy emerges as the most promising technology for further exploration and implementation in Egypt.

1.3 Solar Desalination

Utilizing solar energy as the primary heat source for the evaporation process of saline water, followed by condensation, can be categorized into two main types: direct and indirect solar desalination methods.

1.3.1 Direct Solar Desalination

In direct solar desalination systems, solar radiation is directly converted into heat, which is then used to evaporate saline water within the same device. Examples of such systems include solar stills and humidification-dehumidification systems [6], [7].

Solar stills replicate a natural hydrologic cycle on a smaller scale. The basic design resembles that of a greenhouse as seen in Fig. 1.2 [8]. Solar energy penetrates the device through a sloping transparent panel made of glass or plastic, heating a basin containing saline water. Typically, the basin is coated black to enhance energy absorption. As the water heats up, it evaporates and subsequently condenses on the cooler surface of the glass or plastic panels. The condensed droplets then run down the panels and are collected as freshwater for use.

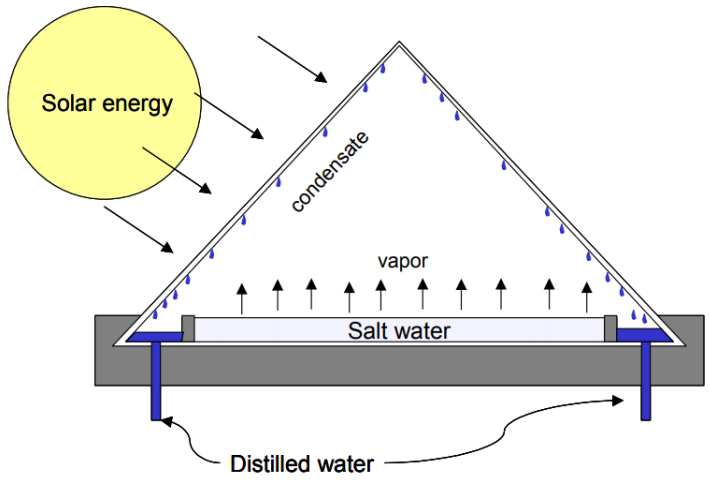

Fig. 1.2 Solar still.

1.3.2 Indirect Solar Desalination

Indirect solar desalination systems comprise two distinct subsystems: a conventional desalination unit and a solar collector. In these systems, solar radiation is initially absorbed by the solar collector and then transferred to the saline water undergoing desalination in the desalination unit, either as heat energy or converted into electric energy.

For desalination units employing distillation techniques, coupling options include flat collectors, evacuated tubes, or solar concentrating collectors. Conversely, desalination units utilizing membrane techniques are typically coupled with Photovoltaic (PV) technology [7], [8], [9].

1.3.2.1 Solar Concentrating Collector

Solar concentrating collectors are optical systems designed to concentrate solar radiation falling on their aperture area onto a receiver positioned at their focal point. This concentration enables higher temperatures to be achieved with a smaller absorber surface area [10]. Concentration can be accomplished through either reflection using mirrors or refraction using lenses.

Linear Fresnel reflectors, Parabolic trough collectors, and Parabolic dish reflectors are all examples of solar concentrating technologies, the specifications for each technology can be found in Table 1.1.

Table 1.1 Solar concentrating collectors [11].

Motion	Collector Type	Absorber Type	Concentration Ratio	Temperature Range (°C)
Single axis tracking	linear Fresnel reflector	Tubular	10-40	60-250
	Parabolic trough collector	Tubular	15-45	60-300
Dual axis tracking	Parabolic dish reflector	Point	100-1000	100-500

The parabolic dish concentrator features a singular focal point and employs mirrors or reflective foils for reflection. It is essential for the concentrator to have dual-axis tracking, allowing adjustments to the azimuth and elevation angles to align precisely with the sun for optimal DNI on the solar dish concentrator (SDC) [12]. Compared to other concentrators, the parabolic dish demonstrates superior performance, capable of achieving elevated temperature ranges and high concentration ratios [13]. Additionally, it exhibits low thermal losses, leading to high thermal and optical efficiencies [14]. Furthermore, it can be integrated into hybrid systems by combining it with other devices [15].

1.4 Thesis Outline

The thesis is organized into six main sections, systematically presenting the research conducted from the background study to the final conclusions and recommendations.

- **Chapter 1: Introduction**

  This section introduces the global issue of water scarcity and the significance of efficient freshwater production methods, highlighting the potential of solar desalination. It articulates the specific problem addressed, outlining the limitations of existing solar still technologies and the potential benefits of the proposed system. The research objectives are presented, and an overview of the thesis structure provides a roadmap for the reader.

- **Chapter 2: Literature Review**

  This section reviews existing solar still technologies, their operation principles, and limitations, focusing on the advantages of concentrated solar stills. It also discusses innovations explored in previous research, such as the use of energy storage materials and nanoparticles to improve the performance of conventional solar still.

- **Chapter 3: Experimental Setup**

  This section describes the design of the sun-tracking concentrated solar still, including the parabolic dish, tracking mechanism, and solar still components. It details the construction process, materials used, and instruments for measuring key performance parameters.

- **Chapter 4: Experimental Procedure and Analysis**

  This section explains the experimental scenarios, such as varying feed water salinity and filling ratios. It outlines procedures for data collection during experiments and methods for analyzing the collected data, including statistical techniques and performance metrics calculation.

- **Chapter 5: Results and Discussion**

  This section presents experimental results, including hourly production, daily cumulative productivity, and system efficiency. It analyzes the effects of feed water salinity and filling ratios on solar still performance and compares the proposed system’s performance with conventional solar stills. It also evaluates freshwater production cost.

- **Chapter 6: Conclusion and Future Work Recommendation**

  This section summarizes key research findings, highlighting the study's achievements and contributions. It draws conclusions based on results and discussions, addresses the research objectives, and suggests further research and development to build on this study's findings, including potential improvements and new investigation areas.

The final part of the thesis includes a comprehensive list of references cited throughout the work, followed by appendices that provide supplementary information. Additionally, an Arabic abstract is provided.

CHAPTER 2

LITERATURE REVIEW

2.1 Introduction

In the ongoing pursuit of securing freshwater for essential daily needs such as drinking and agriculture, extensive research has been conducted to enhance water desalination systems and augment their efficiency. These investigations have encompassed various desalination techniques, with particular emphasis on advancements in solar still systems. Research efforts have focused on material and structural modifications, as well as innovative enhancements aimed at increasing evaporation rates (such as fins, wicks, phase change materials, etc.…), and optimizing solar radiation absorption through the utilization of solar concentrator collectors.

This chapter presents a comprehensive review of previous research about solar still system performance and modifications, organized into three distinct sections. The first section examines traditional solar still configurations and explores diverse enhancements designed to increase productivity. Subsequently, the second section explores the utilization of solar parabolic troughs in conjunction with solar still systems. Finally, the third section addresses the impact of implementing solar dish concentrators on solar still efficiency.

2.2 Conventional Solar Still

El-Sebaey et al. [16] conducted a study to investigate the impact of water depth on the performance of a single-slope solar still with a basin area of 1 m^2 and 23° slope for a glass cover during the summer season, utilizing both empirical and analytical approaches. The findings revealed that as the water depth increased from

2 cm, the cumulative output decreased by 15.41%, 27.17%, and 33.33% for water depths of 3 cm, 4 cm, and 5 cm, respectively.

Manokar et al. [17] investigated the impact of water depth on the productivity of a pyramid solar still with a basin area of 0.25 m^2 made of galvanized iron sheet through experimental means. The study revealed that compared to a water depth of 1 cm, the cumulative productivity decreased by 8.6%, 27.42%, and 44.09% for water depths of 2 cm, 3 cm, and 3.5 cm, respectively.

Maridurai et al. [18] evaluated to assess the impact of water depth (10, 20, 30 mm) and the addition of 30 kg of PCM (paraffin wax) on a double slope solar still with a basin area of 1.5 m^2 with a 17° tilt angle of the glass cover. In addition, a flat plate solar collector was coupled to preheat the water before entering the solar still. The findings indicated that as the water depth decreased, productivity increased. Furthermore, the inclusion of PCM enhanced the distilled yield by 22% at an optimal water depth of 10 mm.

Panchal et al. [19] experimentally demonstrated the impact of incorporating black paint mixed with graphite powder on the absorber plate on the solar still productivity. It was found that the addition of graphite powder resulted in increased productivity compared to CSS by 10.5% and 17% for weight fraction concentrations of 20% and 40%, respectively.

Rahmani et al. [20] conducted experimental investigations to examine the impact of an external condenser on the performance of a solar still. The external condenser, comprising a 0.29 m^2 galvanized sheet with 5 vertical aluminum tubes attached to the rear wall of the solar still, was evaluated. The results revealed that the addition of an external condenser does not consistently yield positive effects, with the performance being dependent upon weather conditions. Specifically, in

moderate weather conditions, the external condenser improved solar still productivity by 29%. However, in excessively hot or cold weather, it led to a decrease in productivity by 16.5%.

Thakur et al. [21] investigated the influence of CuO nanoparticles on the performance of a single slope solar still with a basin area of 1 m^2, which was tested with a constant water depth of 4 cm. The study revealed that the incorporation of CuO nanoparticles led to an increase in distilled yield by 32.67% and 68.9% during winter (with a tilt angle of 41°) and summer (with a tilt angle of 11°), respectively, compared to CSS.

Dhivagar et al. [22] experimentally assessed the performance of a solar still utilizing energy storage biomaterial, specifically conch shells. The solar still, constructed from a carbon steel plate with an area of 0.5 m^2 and a 15° glass cover slope, incorporated 60 black-painted conch shells spread across the basin. The study demonstrated that employing conch shells led to a cumulative productivity increase of 10.8% compared to CSS. Additionally, it enhanced energy and exergy efficiencies by 10.3% and 9%, respectively.

Alshqirate et al. [23] conducted experimental investigations to explore the enhancement of solar still productivity through the utilization of energy storage natural fibers, specifically palmately leaf. A pyramid solar still consisting of a stainless steel basin with a 1 m^2 area, filled with 1.3 kg of palmately leaf material was employed. The study revealed significant improvements, with the cumulative productivity and thermal efficiency increased by 44.5% and 44.8%, respectively, compared to CSS.

Shah et al. [24] utilized black gravel as an energy storage medium in a single slope solar still, featuring a basin with dimensions of 1010 mm in length, 325 mm

in width, and a tilt angle of 20°. The implementation of black gravel resulted in a notable enhancement, with the distilled output increased by 10-17%, achieved at minimal additional cost.

Tiwari et al. [25] employed OM 37, an organic chemical-based PCM with a nominal melting temperature of 37 °C, in a single slope solar still. The solar still featured a basin area of 0.4 x 0.3 m^2, with a glass cover inclined at 26.84°. Two structural configurations were tested: one with the PCM circulated through copper pipes, and the other with the PCM placed beneath a copper sheet. Compared to CSS, these modifications led to significant enhancements in cumulative productivity, with improvements of 21.7% and 29.4%, respectively.

Jahanpanah et al. [26] conducted experimental investigations to examine the impact of low-temperature PCM 28/315 (salt hydrate) on the performance of CSS. The CSS featured a square stainless-steel basin with a glass slope inclined at 35°. Utilizing 3 kg and 6 kg of PCM resulted in overall productivity enhancements of 8% and 30.3%, respectively, compared to conventional setups. Furthermore, employing 6 kg of PCM led to an efficiency improvement of 8.29% relative to CSS.

Al-Harahsheh et al. [27] conducted experimental investigations to explore the impact of connecting a solar collector and utilizing PCM on the performance of a solar still. The solar still basin, constructed from black-painted stainless steel, had an area of 0.83 m^2 and featured a glass cover with a tilt angle of 35°. Additionally, 26 stainless steel tubes, each with a diameter of 3.2 cm, were filled with PCM and submerged in the water basin. A flat plate solar collector was connected to the solar still via a copper coiled tube. The findings revealed that the addition of a solar collector increased productivity by 340%. Furthermore, incorporating PCM into the system resulted in an additional 50% enhancement in productivity compared to the solar collector alone.

Sharshir et al. [28] investigated the impact of incorporating reflectors on the productivity of a pyramid solar still with a basin area of 0.64 m^2. The solar still was equipped with four external movable reflectors, which could be adjusted to optimize the reflection of solar radiation into the solar still. The findings revealed a significant enhancement in productivity, with a 52% increase attributed to the use of reflectors.

2.3 Solar Still Coupled with Parabolic Trough

Additionally, to further enhance the productivity of the solar still, integration with solar concentrators has been explored. For instance, the parabolic trough concentrator is employed to concentrate the incident radiation onto its aperture area, directing it to the focal line where the receiver is positioned to absorb the concentrated heat.

Abdel-Rehim and Lasheen [29] conducted a comparison between the effects of coupling an 80 cm long stainless steel parabolic trough, utilizing oil as a thermal fluid, to elevate the temperature of saline water in a solar still and a CSS, both with a basin area of 1 m. The parabolic trough was covered with transparent plastic to minimize heat loss, employing the greenhouse effect. The findings revealed that the modified solar still exhibited an average increase of 18% in distilled water productivity compared to CSS.

H. Amiri et al. [30] developed a theoretical model of a solar still with dimensions of 60 cm x 10 cm x 38 cm, positioned at the focal point of both stationary and tracked parabolic troughs. The model was tested with a constant 4 cm water depth in the basin and evaluated under Iran's winter weather conditions. The model was validated using experimental results and utilized to assess the impact of four seasons and fixed or tracking troughs on productivity. The findings indicated that the distilled water yield during summer was 0.961 L, which represents a 55%

increase compared to winter, for a fixed parabolic trough with a slope of 60°. Additionally, for a tracking trough, the yield during summer was 1.266 L, which represents a 70% increase compared to winter conditions.

Elashmawy [31]-[34] conducted a study that involved integrating a tubular solar still with an area of 0.059 m^2 with a parabolic trough solar tracking system featuring a projected area of 0.87 m^2. The findings indicated a significant improvement in daily yield by 676%, accompanied by a reduction in the CPL by 45.5% due to the integration of the parabolic trough [31]. The study further explored the impact of cooling methods on the system's performance. Two cooling strategies were assessed: spraying over the tubular solar still and employing concentric tubes for cooling. The results revealed that both approaches led to a decrease in productivity by 10% and 43.8%, and a reduction in efficiency by 7.79% and 42.63%, respectively [33]. Additionally, the study investigated the use of black gravel as a sensible energy storage material, which resulted in an enhancement of productivity and efficiency by 14.18% and 13.89%, respectively [32]. Lastly, the incorporation of a parabolic trough to the tubular solar still, combined with Calcium Chloride desiccant for water harvesting in low humid regions, yielded remarkable improvements in productivity and efficiency by 292.4% and 82.3%, respectively, while simultaneously reducing the CPL by 25% [34].

Essa et al. [35] conducted experimental research on a tubular solar still featuring a rotating drum with dimensions of 100 cm in length and 50 cm in diameter. The impact of incorporating nanoparticles (CuO), a parabolic solar concentrator with a rim angle of 40º and an aperture width of 150 cm, as well as PCM (paraffin wax) on its performance, was investigated. The productivity enhancements over CSS were found to be 137%, 185%, and 208% for the cumulative addition of nanoparticles, parabolic solar concentrator, and PCM,

respectively. The CPL of the modified tubular solar still and CSS were calculated to be 0.024 $/L and 0.029 $/L, respectively, while the payback period was determined to be 5 months and 3 months, respectively.

Alqsair et al. [36] conducted an experimental study aimed at enhancing the performance of drum solar still with a projected area of 0.5 m^2, equivalent to a CSS. The effects of incorporating nanoparticles (Ag), a parabolic solar concentrator with a rim angle of 40º and an aperture width of 150 cm, as well as PCM (paraffin wax) on the performance of the solar still was investigated. The study revealed significant productivity enhancements over CSS, with improvements of 221%, 262%, and 294% observed for the cumulative addition of nanoparticles, parabolic solar concentrator, and PCM, respectively. Furthermore, the CPL of the modified drum solar still and CSS were calculated to be 0.023 $/L and 0.029 $/L, respectively, while the payback period was determined to be 134 and 172 days, respectively.

2.4 Solar Still Coupled with Solar Dish Concentrator

Furthermore, the dish represents another category of solar concentrator, which redirects incident radiation received on its aperture area into a focal point, thereby achieving elevated temperature ranges and concentrator ratios.

Chaouchi et al. [37] designed and constructed a desalination unit utilizing an SDC with a concentration ratio of 195. Also developed a theoretical model to assess its performance. The comparison between experimental and theoretical outcomes indicated minimal disparity in absorber average temperature. However, theoretically, the unit was projected to produce 10.4 liters with an average relative error of 42%, attributed to manual tracking and paraboloid geometry.

Prado et al. [38] conducted experimental and theoretical investigations into the performance of an SDC for water desalination. A glass flask positioned at the

focal point of the satellite dish, with mirrors serving as reflectors was utilized. Various salinity concentrations (ranging from 0% to 4%) were tested, leading to the deduction that productivity decreased with increasing salinity. The study revealed maximum and minimum freshwater production rates of 4.95 kg/m^2.day and 4.11 kg/m^2.day, respectively, achieved at salinity concentrations of 0% and 4%.

Gorjian et al. [39] constructed a point-focus parabolic solar still coupled with two plate heat exchangers, intended for preheating saline water and condensing steam. The parabolic dish had a diameter of 2 m, featuring an absorber made of steel alloy with an area of 0.031 m^2 and a geometrical concentration of 100, while the heat exchangers had an area of 0.14 m^2 each. The tested device achieved a maximum daily productivity of 5.12 kg/day and an efficiency of 36.7%. The cost of distilled water produced by the device was determined to be 0.012 $/kg.

Omara and Eltawil [40] designed a novel system incorporating a boiler positioned at the focal point of an SDC. They assessed the impact of adding water preheating on system performance and compared it to CSS. The SDC demonstrated significant enhancements in distillate water production compared to CSS, achieving improvements of 244% and 347% without and with preheating, respectively. Furthermore, the average daily efficiencies of SDC with preheating and CSS were determined to be 68% and 34%, respectively. The average CPL of distilled water produced by SDC with preheating was calculated to be 0.028 $/L, whereas for CSS, it was 0.048 $/L.

Bahrami et al. [41] conducted experimental and theoretical investigations on an SDC with a solar still mounted at its focal point and validated the proposed mathematical model using experimental data. Various parameters were explored, leading to the conclusion that the initial temperature of saline water, salinity, and the mass of saline water in the evaporator had no significant effect on system

performance. However, for a dish with an aperture diameter of 2 m, decreasing the reflectivity of the absorber plate from 0.7 to 0.4 and increasing the optical efficiency of the dish from 0.5 to 0.8 resulted in an increase in distilled water production by 120% and 80%, respectively.

Abubakkar et al. [42] constructed an SDC utilizing aluminum foil as a reflector, with a diameter measuring 1.46 m. A solar still, measuring 33 cm in length and 19 cm in width, was mounted at the focal point of the dish. Water properties were tested before and after the desalination process. The experiment successfully decreased the salinity from 23750 to 50 ppm and adjusted the pH from 7.55 to 7, yielding only 65 mL of distilled water.

Al-Qasaab et al. [43] improved the efficiency of a solar still by integrating it with an SDC and investigating the impact of employing a copper helical conical coil on the condensation rate. Both the SDC and the solar still were constructed from galvanized steel, with areas of 1.76 m^2 and 0.045 m^2, respectively. The copper conical coil comprised 6 coil loops, measuring 0.15 m in height and 3.5 m in length. The productivity was enhanced from 8.2 to 11.45 L/day by incorporating the coil, resulting in a 39.6% increase. The daily average freshwater output reached 10.5 L/day, leading to an average annual production of approximately 3360 L/year.

Tawfik et al. [44] conducted both experimental and numerical investigations into the impact of saline water mass and water salinity on a novel solar dish desalination system. This system involved utilizing a vessel as a boiler, which was inserted into a glass box to minimize heat losses. In the numerical analysis, using a saline water mass of 0.75 kg and varying salinity from 0 to 200 ppt, the daily distilled water yield decreased from 500 to 320 mL/m^2, and the efficiency dropped from 88.6% to 19%. Meanwhile, in the experimental study, under the optimal conditions with a salt concentration of 15 ppt and 0.75 kg of saline water, the daily accumulated

productivity and efficiency were 13.27 mL/m^2 and 36.04%, respectively, with a CPL of 0.64 $.

Srithar et al. [45] conducted an experimental study to investigate the impact of an SDC, cover cooling, and PCM on the productivity of a triple basin solar still. The triple basin was constructed using 4 mm thick glass, with a basin area of 0.108 m^2, positioned at the focal point of a 1.25 m dish made of aluminum. The utilization of charcoal and river sand as PCM led to a productivity enhancement of 34.28% and 25.71%, respectively. Additionally, cover cooling increased productivity by 30%. Integrating the triple basin solar still with an SDC, charcoal, and cover cooling resulted in a productivity of 16.94 kg/m^2.day, showcasing a remarkable 161% enhancement compared to the triple basin solar still alone. The CPL of distilled water produced by this combined system was 0.084 $.

Arunkumar et al. [46] conducted an experimental investigation to analyze the impact of cover cooling at various flow rates (0, 40, 50, 60, 80, 100 mL/min) and the use of paraffin wax PCM on the productivity of a solar still positioned at the focal point of an SDC. The solar still featured six copper balls filled with 25 g of PCM, situated within a hemispherical copper absorber with a diameter of 0.22 m and a glass cover inclined at 11°. The findings demonstrated a direct relationship between productivity and cooling water flow rate; however, this approach was deemed less cost-effective. Conversely, the utilization of PCM was found to enhance productivity cost-effectively. Specifically, at a cover cooling flow rate of 100 mL/min, the daily productivity reached 3.8 L when PCM was employed.

2.5 Literature Review Summary

In the reviewed literature, various experimental and numerical studies have been conducted, revealing several key findings and trends:

- Solar stills utilizing solar concentrators are significantly more effective compared to conventional solar stills. The concentrators' ability to provide increased radiation and achieve higher temperatures contributes to enhanced productivity, all while maintaining a relatively small absorber area.
- The majority of research on concentrated solar stills has centered around parabolic troughs. These studies have explored different configurations and operating parameters to optimize performance. The findings indicate that parabolic troughs can effectively increase the efficiency and productivity of solar stills.
- There is a noticeable gap in the literature regarding the use of concentrated solar stills with solar dishes under various operating conditions. Additionally, no studies have been conducted on the implementation of tracking solar dishes, particularly those with automatic tracking systems. This represents a significant area for potential future research.
- Several modifications have been investigated to improve the performance of conventional solar stills. For instance, the incorporation of energy storage materials has been shown to extend the production duration of solar stills. Furthermore, the addition of nanoparticles to black paint covering the absorber plate or to the water in the basin has been found to enhance heat transfer and improve evaporation rates.

Overall, the literature indicates a strong potential for concentrated solar stills to outperform conventional designs, particularly with further research and development focused on solar dish applications and advanced tracking mechanisms.

2.6 Thesis Objectives

This research aims to address several critical objectives in the field of solar desalination, with a focus on improving the efficiency and effectiveness of solar stills through innovative design and operational strategies. The specific objectives of this thesis are as follows:

- Development a novel Sun-Tracking Concentrated Solar Still system: To design, construct, and experimentally evaluate its performance. This system will utilize a dual-axis tracking mechanism to maximize solar energy capture and enhance the overall performance of the solar still.
- Evaluation of Key Performance Parameters: To systematically investigate the effects of varying key parameters on the performance of the concentrated solar still. These parameters include the salinity of the feed water and the filling ratio of saline water within the solar still. Also determine the optimal conditions for maximizing distilled water productivity and system efficiency.
- Comparative Analysis with Conventional Solar Stills: To conduct a comparative analysis between the proposed concentrated solar still and conventional solar stills. This analysis will focus on metrics such as daily cumulative productivity, system efficiency, and the cost of freshwater production. The goal is to quantify the advantages and disadvantages of using a concentrated solar still system over the conventional method.
- Assessment of Economic Feasibility: To assess the economic feasibility of the proposed concentrated solar still by analyzing the cost of freshwater

production and comparing it with other desalination technologies. To demonstrate the potential for widespread adoption of this technology in regions with limited access to freshwater.

By achieving these objectives, this research aims to contribute significantly to the advancement of solar desalination technologies, providing a viable and sustainable solution for addressing water scarcity in arid and semi-arid regions.

CHAPTER 3

EXPERIMENTAL SETUP

3.1 Introduction

This chapter outlines the test rig, its components, and the experimental setup objectives. The primary aim of this study is to examine the impact of salinity and the quantity of saline water in the evaporator on the productivity of a solar still positioned at the focal point of a solar dish concentrator. The experimental setup is located on the rooftop of the Rod El-Farag building at the Shoubra Faculty of Engineering, Benha University.

3.2 Experimental Setup

A water desalination experimental setup was conceived and constructed, comprising two primary sections: the solar dish concentrator and the solar still. The solar dish concentrator section incorporates the solar dish itself, a dual-axis tracking controller, and two actuator motors. Meanwhile, the solar still section encompasses the solar still apparatus, a saline water tank, a pump, flexible hoses for connection, and a drain hose. Various measuring instruments were utilized in this study, including K-type thermocouples, a data acquisition (DAQ) system, a thermal imager, a thermometer, a solar power meter, a weather station, a salinity meter, a graduated cylinder, and a weighing balance.

The layout of the experimental setup is depicted in the schematic diagram presented in Fig. 3.1. Table 3.1 provides a list naming the main components of the experimental test rig. Additionally, Fig. 3.2 offers a pictorial view of the experimental setup, providing a real picture of the apparatus.

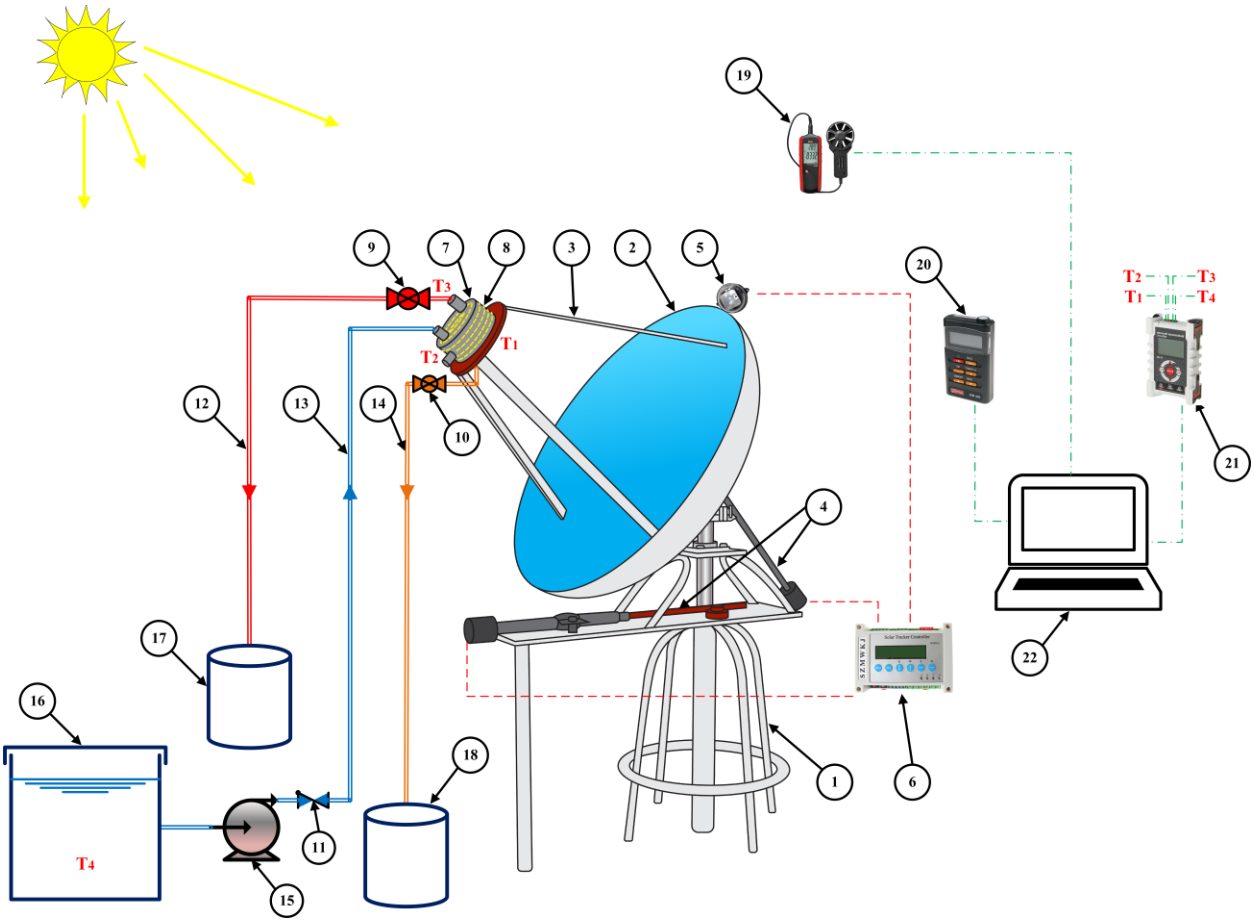

Fig. 3.1 A layout of the experimental setup.

Table 3.1 The experimental test rig's main components.

Item No.	Component description	Item No.	Component description
1	Supporting Frame	12	Vapor Hose
2	Solar Dish Concentrator	13	Makeup Hose
3	Holding Arms	14	Drain Hose
4	Dual-Axis Tracking System	15	0.3 HP Centrifugal Pump
5	Sun Tracking Sensor	16	Saline Water Tank
6	Sun Tracking Controller	17	Distilled Water Tank
7	Solar Still	18	Brine Tank
8	1 inch Glass Wool Insulation	19	Digital Anemometer
9	1 inch Ball Valve	20	Digital Solar Power Meter
10	½ inch Ball Valve	21	Data Acquisition System
11	½ inch Check Valve	22	Laptop

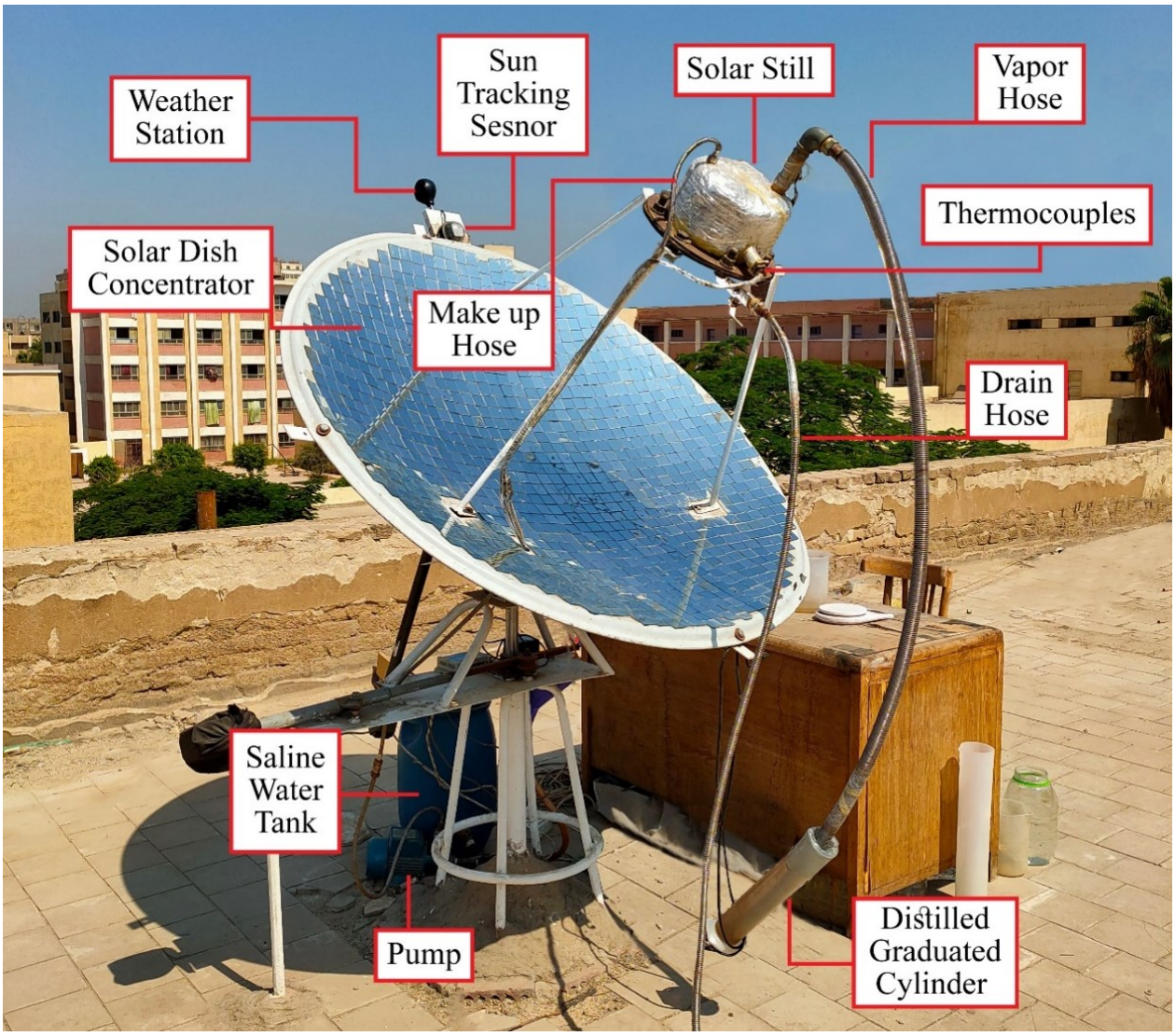

Fig. 3.2 Sun-tracking concentrated solar still experimental setup.

3.2.1 Solar Still

The solar still is constructed from stainless steel to prevent the deposition of salts and impurities on its inner walls. It features a cylindrical shape with a diameter of 0.2 m and a height of 0.12 m, while its flange diameter measures 0.34 m and is affixed to the absorber plate as shown in Fig. 3.3. The absorber plate, crafted from copper with a diameter of 0.34 m and a thickness of 0.003 m (3 mm), is coated with

a black solar-selective coating (Krylon) to enhance absorption and minimize reflection. To minimize heat loss to the surroundings, the solar still is enveloped in 0.025 m (25 mm) thick glass wool insulation. The detailed specifications of the insulation material are provided in Table 3.2.

Table 3.2 Specifications of glass wool insulation.

Density	16 kg/m^3
Thickness	25 mm
Heat conductivity	0.038 W/m.k
Highest usage temperature	450 °C

Four ports are integrated into the solar still: two at the top—one serving as the inlet for saline water makeup and the other as the outlet for vapor passage. A third port is positioned in the side wall for thermocouple insertion, while the final port, located in the absorber plate, facilitates the drainage of brine.

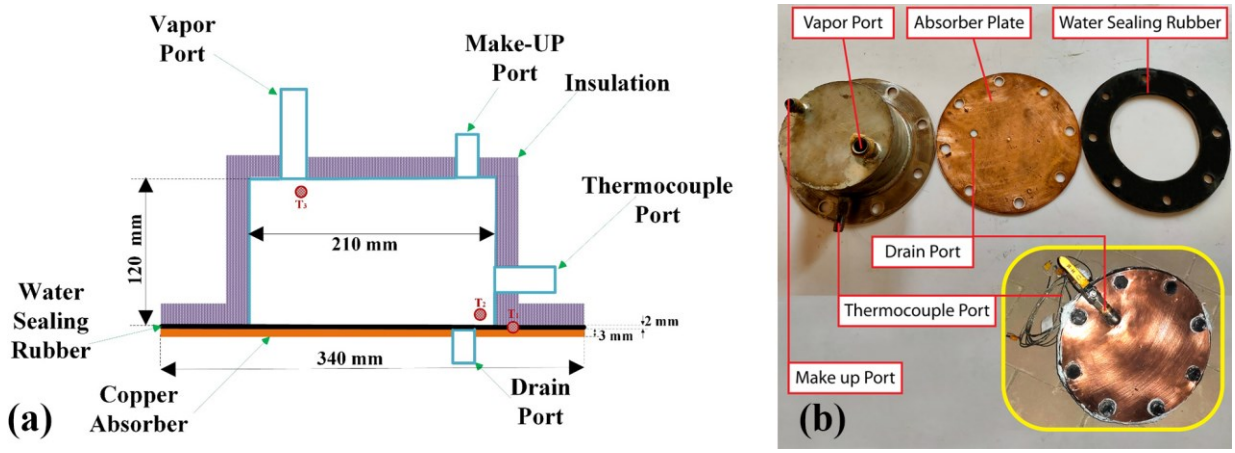

Fig. 3.3 cylindrical solar still, (a) detailed schematic diagram, (b) actual photo.

3.2.2 Solar Dish Concentrator

The solar dish concentrator (SDC) is constructed from steel with a thickness of 2 mm and features an aperture diameter of 1.2 m. Reflective mirrors, each measuring 0.05 m x 0.05 m, are square segmented and affixed onto the SDC to

redirect solar radiation toward its focal point shown in Fig. 3.4. The solar still is mounted at this focal point using three steel holding rods, each with a length of 0.77 m, ensuring stability and proper alignment.

Fig. 3.4 Solar dish concentrator.

3.2.3 Sun Tracking System

A dual-axis tracking system was implemented to ensure precise alignment of the SDC with the incident solar rays. This system operated in two stages: first, an actuator positioned horizontally on the base, welded to a rack interlocked with a pinion on the axis of the movable base of the SDC. This arrangement allowed the SDC to rotate horizontally with a freedom of 225 degrees, facilitating adjustment of the solar azimuth angle. Second, another actuator was attached to the SDC and a

point on the movable base, enabling rotation on four vertical flange bearings to control the elevation angle of the SDC as illustrated in Fig. 3.5a. This adjustment aimed to optimize the angle for maximum DNI on the SDC.

These actuators were connected to a solar tracker controller (WST03-2), powered by a 24 Volt AC/DC adaptor. The controller utilized dust and water-proof sensor composed of four small photovoltaic (PV) panels, each directed towards a different direction, with a sun-visor positioned on top to regulate radiation exposure as depicted in Fig. 3.5b. These sensors generated varying voltage values corresponding to the solar radiation received from different directions. The voltage data was then transmitted to the main board via a five-core cable, where it was analyzed to determine the optimal positioning of the SDC relative to the sun's radiation. Based on this analysis, control commands were sent to the actuators to ensure precise alignment with the sun's rays.

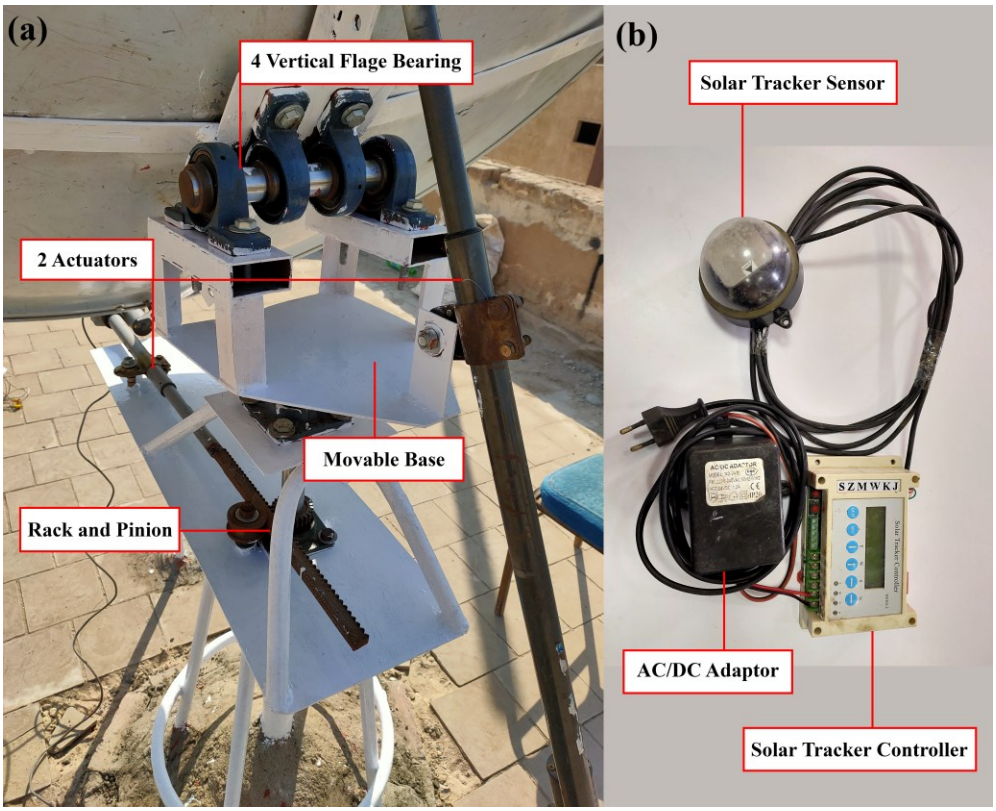

Fig. 3.5 (a) Dual-axis tracking mechanism, (b) Solar tracker controller.

3.2.4 Pump

A 0.3 HP centrifugal water pump as presented in Fig. 3.6 is employed to supply water from the saline water tank to the solar still whenever the mass of saline water inside the solar still falls below the pre-set value for the specific test day. Saline water is manually pumped into the solar still whenever the distilled water produced reaches 25% of the initially charged saline water.

Fig. 3.6 Centrifugal water pump.

3.2.5 Flexible Connections

Two types of flexible connections are utilized in the setup. The first type is composed of rubber with a nickel shield as visualized in Fig. 3.7a, featuring a diameter of 0.5 inches. This highly flexible setup includes a connection from the saline water tank to the pump and another connection from the pump to the solar still.

The second type of flexible connection is constructed from stainless steel shown in Fig. 3.7b and comes in two sizes: 0.5 inches for drainage purposes and 1 inch for vapor transfer, which also serving as a condenser for the solar still due to its unique finned shape.

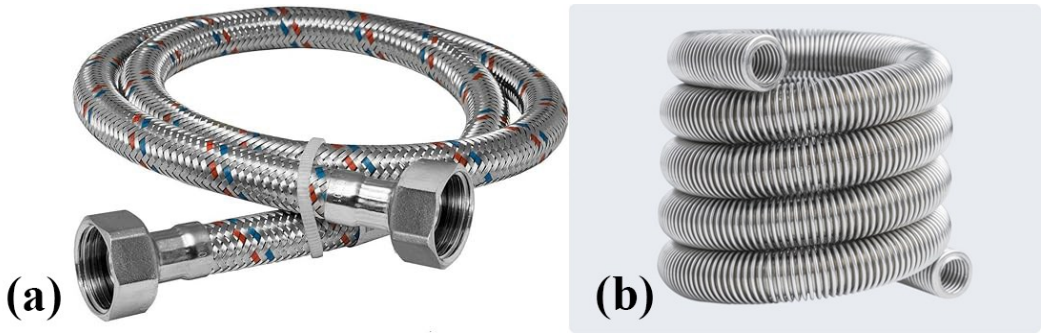

Fig. 3.7 Flexible connections (a) rubber with a nickel shield, (b) stainless steel.

3.2.6 Valves

Two types of valves are incorporated into the setup. The first is a horizontal lift check valve, constructed from bronze Fig. 3.8a, which prevents backflow to protect the pump.

The second type is a ball valve Fig. 3.8b, available in two sizes: a 0.5 inch valve installed on the drain hose, typically closed except during drainage, and a 1 inch valve placed on the vapor hose, which remains open under normal operation.

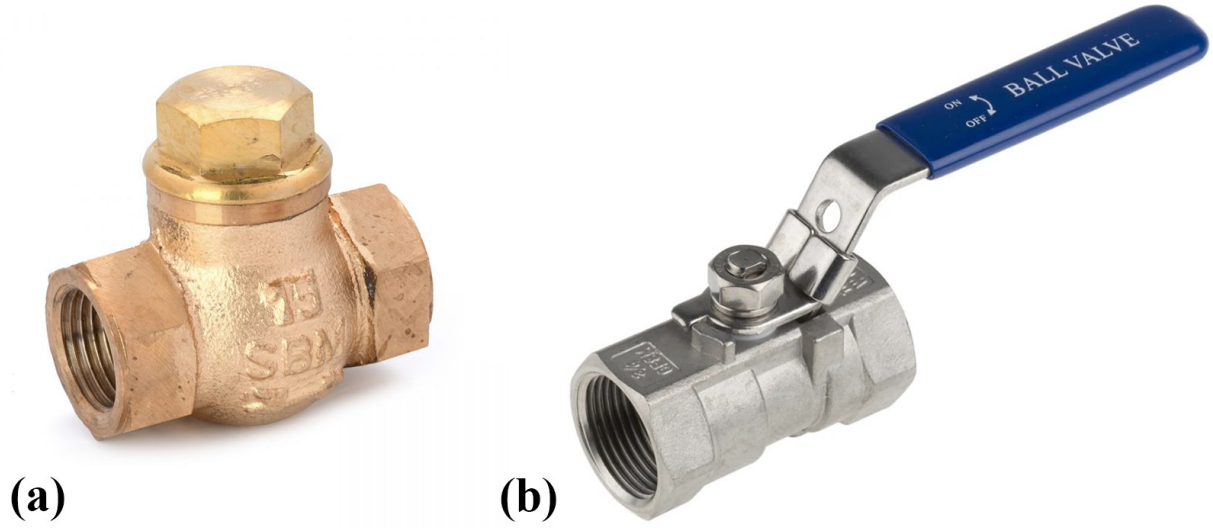

Fig. 3.8 Valves (a) check valve (b) ball valve.

3.3 Measurement Instruments

3.3.1 Temperature Measurement

3.3.1.1 Thermocouple

Temperature readings inside the solar still are obtained using K-Type (MAX6675) thermocouples equipped with stainless steel probes as visualized in Fig. 3.9a. Three thermocouples are strategically placed within the solar still to measure various parameters: the temperature of the absorber plate, the temperature of the saline water in the evaporator, and the temperature of the vapor generated. These thermocouples are connected to a multichannel recorder (MCR-4TC) data logger depicted in Fig. 3.9b, which displays the instantaneous temperatures of the connected thermocouples on its screen. Additionally, the data logger is equipped with the capability to record the temperature data onto SD card. The recorded data can later be downloaded to a computer and using the program that named (T&D Graph) which a graphical software for viewing and analyzing data recorded by the data logger.

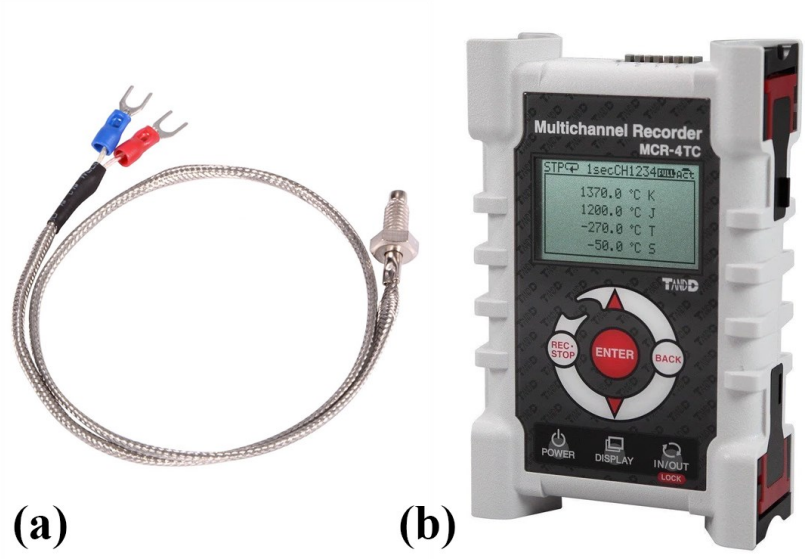

Fig. 3.9 (a) Thermocouple, (b) multichannel recorder data logger.

3.3.1.2 Thermal Imager

The external temperature of the absorber was measured using a (Fluke Ti32) thermal imager shown in Fig. 3.10, known for its high-resolution imaging abilities. With its 320x240 pixels sensor, this thermal imager captures clear images, allowing it to identify even the smallest temperature differences with precision.

Fig. 3.10 Thermal imager.

3.3.1.3 Thermometer

Temperature readings for the saline water in the tank and the distilled water product were obtained using a thermometer shown in Fig. 3.11. The specifications of this thermometer are presented in Table 3.3.

Table 3.3 Specifications of thermometer.

Model	Mercury glass thermometer
Range	-10−120 ℃
Accuracy	± 0.5 ℃
Display	Analog

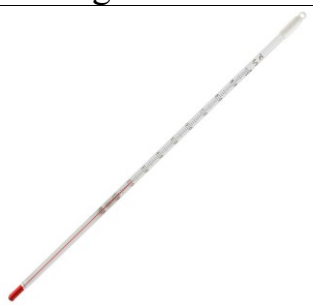

Fig. 3.11 Thermometer.

3.3.2 Solar Power Meter

The direct normal irradiance at the experiment location was measured using a (TES-1333R) data logging solar power meter depicted in Fig. 3.12. This meter was installed and fixed on the surface of the solar dish concentrator. The specifications of this meter are presented in Table 3.4.

Table 3.4 Specifications of the solar power meter.

Model	TES-1333R
Range	0–2000 W/m^2
Display	4 digits
Accuracy	± 5% of reading or ±10 W/m^2 whichever is high in sunlight
Drift	< ± 2% per year
Angular accuracy	Cosine corrected < 5% for angles < 60º
Over-input	The display shows "OL"
Sampling rate	4 times/sec
Dimensions	110 x 64 x 34 mm
Operating temperature and humidity	0°C ~ 50°C, below 80% RH
Weight	Approx. 158 g

Fig. 3.12 Solar power meter.

3.3.3 Salinity Meter

Samples of the saline water were prepared, and their salinity was measured using the (AD410) TDS-TEMP portable meter visualized in Fig. 3.13. The instrument's auto-ranging feature automatically adjusts the TDS readings to the scale with the highest resolution. The specifications of this meter are detailed in Table 3.5.

Table 3.5 Specifications of salinity meter.

Model	AD410
Range	0-99.9 ppt
TDS Resolution	0.01 ppm from 0 to 9.99 ppm, 0.1 ppm from 10 to 99.9 ppm, 1 ppm from 100-999 ppm, 0.01 ppt from 1 to 9.99 ppt, 0.1 ppt from 10 to 99.9 ppt
TDS Accuracy	± 1%

Fig. 3.13 Salinity meter.

3.3.4 Anemometer

The ambient temperature and wind velocity were recorded utilizing a digital anemometer (WT8907) featuring an auxiliary fan positioned on a retractable handle, as depicted in Fig. 3.14. This fan was situated on the surface of the SDC. The anemometer features a data logger and a reading screen for real-time measurements. Data can be recorded and downloaded to a computer via a USB connection for

further analysis using the accompanying Windows software. The specifications of this meter are outlined in Table 3.6.

Table 3.6 Specifications of anemometer.

Model	WT8907
Temperature range	Range: 0-45 ℃
	Accuracy: ± 1 ℃
	Resolution: 0.1 ℃
Humidity range	Range: 10-90% RH
	Accuracy: ± 5%
	Resolution: 0.1% RH
Wind range	Range: 0-45 m/s
	Accuracy: ± 3%
	Resolution: 0.01 m/s
Air volume range	Range: 0-999900 CFM
	Resolution: 0.001-100
Operating temperature and humidity	0°C ~ 50°C, below 80% RH
Dimension	194 x 73 x 38 mm
Weight	Approx. 395 g

Fig. 3.14 Digital anemometer.

3.3.5 Graduated Glass Flask and Weighing Balance

The distilled water productivity was measured using a graduated cylinder shown in Fig. 3.15a. Additionally, the mass of Sodium Chloride salt added to

freshwater to achieve the desired salinities for testing was adjusted using a weighing balance (SF-400) depicted in Fig. 3.15b. The specifications of this balance are detailed in Table 3.7.

Table 3.7 Specifications of weighing balance.

Model	SF-400
Range	0−10000 g
Accuracy	± 1 gm
Display	LCD
Dimensions	245 x 170 x 35 mm
Weighting platform diameter	147 mm
Weight	Approx. 282 g

(a) (b)

Fig. 3.15 (a) Graduated cylinder, (b) weighing balance.

CHAPTER 4

EXPERIMENTAL PROCEDURE AND ANALYSIS

4.1 Introduction

This chapter outlines the methodology and analytical approaches employed to conduct the experimental investigation in the present study. It encompasses the equations utilized for data reduction and addresses the uncertainties associated with the measuring devices.

4.2 Experimental Procedure

The experimental tests were conducted between June and August 2022, spanning from 8:00 to 18:00, exclusively on sunny days with an average direct solar irradiance ranging from 824.2 to 923.2 W/m^2. In this study, the effectiveness of the concentrated solar still was assessed across three distinct feed water salinities, simulated by dissolving Sodium Chloride in freshwater to mimic Mediterranean water (37 ppt) and Brackish water (27 ppt and 17 ppt). Additionally, each saline water sample prepared was subjected to various filling ratios (Ø), denoting the proportion of saline water within the solar still relative to its volume. Specifically, the solar still was filled with 1, 1.5, 2, and 2.5 kg of saline water, corresponding to filling ratios of 26.5%, 39.8%, 53.1%, and 66.3%, respectively. The experimental configurations are detailed in Table 4.1.

Table 4.1 Experimental test configurations.

No.	Mass (kg) Filling ratio (%)	Feed water salinity (ppt)	Date
1	1 kg → 26.5	17	26/7/2022
2		27	25/6/2022
3		37	18/7/2022
4	1.5 kg → 39.8	17	27/7/2022
5		27	27/6/2022
6		37	19/7/2022
7	2 kg → 53.1	17	28/7/2022
8		27	28/6/2022
9		37	20/7/2022
10	2.5 kg → 66.3	17	1/8/2022
11		27	29/6/2022
12		37	21/7/2022

Each experiment commenced with a meticulous cleaning of the reflecting mirrors of the SDC using a dry microfiber cloth, followed by the application of glass cleaner and thorough wiping. Subsequently, the solar still underwent flushing with freshwater and circulated multiple times to ensure the removal of any residual brine from prior experiments. Once this cleaning process was completed, the saline water sample under examination was pumped into the solar still. All measuring devices were then activated, and a final verification was conducted to ensure that everything was properly set up and ready for the commencement of the experiment.

The experiment commences promptly at 8:00 in the morning, with data collection intervals set at 15-minute intervals throughout the day. Whenever the distilled water collected from the solar still reaches an amount equivalent to 25% of the initially charged saline water volume, an equivalent quantity of saline water is added as make-up. As the day progresses, data collection continues until 18:00, coinciding with sunset. At this point, the tracking system is deactivated, signifying

the conclusion of the experiment. The wastewater is then discharged through the designated drain port, and the solar still undergoes a backwashing process. These procedural steps are consistently repeated for each subsequent experiment.

Throughout the experiment, various parameters are monitored and recorded at 15-minute intervals. These include the temperatures of the ambient air, as well as the internal and external surfaces of the absorber plate. Additionally, measurements are taken for the temperatures of the saline water within the evaporator and the vapor produced, the wind velocity, the direct normal irradiance, and the mass of distilled water yield.

4.3 Data Reduction

The temperatures recorded by multiple thermocouples are averaged to derive the representative temperature readings utilized in subsequent calculations.

To interpret the performance of the concentrated solar still based on the gathered data, a set of fundamental mathematical equations is indispensable.

Among these, the concentration ratio (CR), denoted as the ratio between the dish aperture area (A_{dish}) and the absorber area (A_{abs}), holds paramount importance in the design and construction of solar concentrators, as delineated by Equation (4.1):

$$CR = \frac{A_{dish}}{A_{abs}} \tag{4.1}$$

The incident heat on the aperture area of the SDC is calculated using the following Equation (4.2):

$$Q_{solar} = A_{dish} \times DNI \tag{4.2}$$

The heat concentrated on the absorber plate of the solar still is calculated as a function of the incident heat and is given by Equation (4.3):

$$Q_{conc} = \eta_{conc} \times Q_{solar} \tag{4.3}$$

The concentrator efficiency (η_{conc}), defined as the ratio of heat received by the absorber to the heat incident on SDC, is influenced by the optical characteristics of the materials utilized as well as the shape; it is computed by Equation (4.4) [47]:

$$\eta_{conc} = \rho \times \Gamma \times f_s \tag{4.4}$$

Where ρ represents the reflectivity of SDC mirrors, Γ the intercept factor, and f_s is the shading factor generated by the solar still on SDC mirrors.

The dissipation of heat from the absorber plate to the surroundings occurs via two primary methods: radiation and convection. Radiation heat loss is further categorized into two distinct types: reflected and emitted. The calculations for both reflected and emitted radiation heat losses are determined using Equations (4.5) and (4.6), respectively.

$$Q_{ref} = \rho_{abs} \times Q_{conc} \tag{4.5}$$

$$Q_{emit} = \varepsilon_{abs} \times \sigma \times A_{abs} \times (T_{abs}^4 - T_{amb}^4) \tag{4.6}$$

While the estimation of external convection heat loss from an inclined heated flat plate is accomplished through Equations (4.7), (4.8), (4.9), and (4.10) [48], [49]:

$$Q_{conv} = h \times A_{abs} \times (T_{abs} - T_{amb}) \tag{4.7}$$

$$h = \frac{Nu * K_{air}}{L_c} \tag{4.8}$$

$$Nu = 0.325 \times Re^{0.6255} \times (1 + \sin\theta)^{0.5} \tag{4.9}$$

$$Re = \frac{V_{wind} * L_c}{\nu} \tag{4.10}$$

The useful heat energy entering the absorber is determined by subtracting the calculated heat losses from the concentrated heat, as expressed by Equation (4.11):

$$Q_{useful} = Q_{conc} - Q_{loss} = Q_{conc} - \left(Q_{Ref} + Q_{Emit} + Q_{conv}\right) \quad (4.11)$$

Ultimately, the system efficiency is derived from Equation (4.12):

$$\eta_{Sys} = \frac{m_{distilled} * h_{fg}}{Q_{solar} * \Delta t} \quad (4.12)$$

4.4 Thermocouple Calibration

Calibration is critical in ensuring measurement instruments' accuracy and reliability. It involves comparing the measurements obtained from an instrument with a known standard or reference to identify and correct any deviations. This process typically includes adjusting the instrument to align with the standard, ensuring that subsequent measurements are precise and accurate. Calibration is essential for maintaining the integrity of data in scientific research. Regular calibration of measurement instruments helps achieve consistent performance, minimize errors, and ensure compliance with relevant standards and regulations [50], [51].

All thermocouples were calibrated in the laboratory as a single unit against a mercury-in-glass thermometer, which has an accuracy of ± 0.5 ℃. A well-insulated 2-liter flask was used as the calibrator. For each temperature setting, the thermocouples and the mercury thermometer were placed together in the flask. Readings were taken across the testing temperature range [25 ℃–120 ℃]. The calibration data was then plotted to derive fitted curves. The calibration curves are presented in Appendix A (Fig. A.1).

4.5 Experimental Uncertainty Analysis

All measurements inherently contain errors stemming from factors like experimental setup, laboratory procedures, instrument inaccuracies, and environmental influences. Errors, in this context, refer to the disparities between the measurements taken and the actual values, which are seldom precisely known. Therefore, the goal is to derive the most precise approximation of the true value and simultaneously estimate the associated errors. This analytical process is commonly referred to as uncertainty analysis, which aims to assess the accuracy and precision of data, recognizing the inherent complexities involved in determining precise or absolute values in practical scenarios [52], [53].

Table 4.2 outlines the uncertainties linked with different experimental measuring instruments, including the solar power meter, thermocouples, and anemometer, as indicated by the device datasheets. The Holman's method [54] is employed to assess the overall uncertainty in the experimental data. The total uncertainty in the daily distilled productivity and the daily system efficiency of the experimental findings is determined using Equation (4.13):

$$\omega = \sqrt{(\frac{\partial f}{\partial x})^2 \times \omega_x^2 + (\frac{\partial f}{\partial y})^2 \times \omega_y^2} \tag{4.13}$$

Where ω_x and ω_y are the independent variables uncertainties.

As per the uncertainty equation, the maximum total uncertainty in computing the daily distilled productivity and the daily system efficiency is approximately 0.37% and 1.12%, respectively as calculated in Appendix B.

Table 4.2 Uncertainties and errors for various experimental measurement devices.

Device	**Uncertainty**	**Range**
Solar power meter	± 10 W/m^2	0-2000 W/m^2
Anemometer	± 3%	0-45 m/s
	± 1℃	0-45 ℃
Thermocouples	± 2 ℃	0-1024 ℃
Salinity meter	± 1%	0-99.9 ppt
Weighing balance	± 1 gm	0-10000 gm
Calibrated flask	± 25 mL	0-2000 mL
Solar tracker controller	≤ 1°	

CHAPTER 5

RESULTS AND DISCUSSION

5.1 Introduction

The thermal performance of the concentrated solar still is significantly influenced by both operational parameters and prevailing weather conditions. As mentioned earlier, this study examines operational parameters such as the mass of saline water used to fill the solar still, which remains consistent at 1, 1.5, 2, and 2.5 kg, corresponding to filling ratios of 26.5%, 39.8%, 53.1%, and 66.3%, respectively, as well as varying feed water salinities of 17, 27, and 37 ppt.

In this chapter, the study aims to achieve its objectives by analyzing the impact of these parameters on both the productivity and thermal efficiency of the concentrated solar still system.

The experimental work was carried out during the summer months, from June to August 2022, between 8:00 and 18:00 hr, exclusively on sunny days. The daily average Direct Normal Irradiance (DNI) recorded throughout the 12 experiments ranged from a minimum of 824.2 W/m², observed on one day, to a maximum of 923.2 W/m² on another. Similarly, the daily average ambient temperature varied between 35.3 ℃ and 38.4 ℃, while the daily average wind velocity ranged from 1.14 m/s to 1.49 m/s. These values represent the averaged conditions over the course of each experiment day. The hourly distributions of DNI, ambient temperature, and wind velocity for the experimental period are presented in Fig. 5.1.

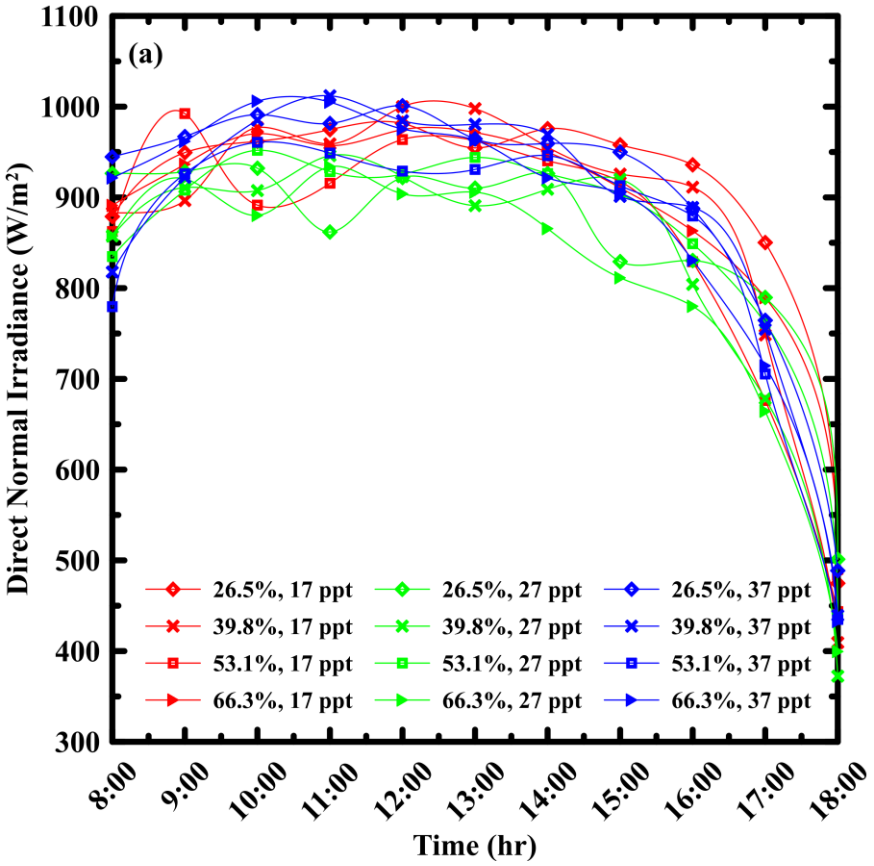
(a)
Direct Normal Irradiance (W/m²)
1100
1000
900
800
700
600
500
400
300
8:00
9:00
10:00
11:00
12:00
13:00
14:00
15:00
16:00
17:00
18:00
Time (hr)
26.5%, 17 ppt
26.5%, 27 ppt
26.5%, 37 ppt
39.8%, 17 ppt
39.8%, 27 ppt
39.8%, 37 ppt
53.1%, 17 ppt
53.1%, 27 ppt
53.1%, 37 ppt
66.3%, 17 ppt
66.3%, 27 ppt
66.3%, 37 ppt

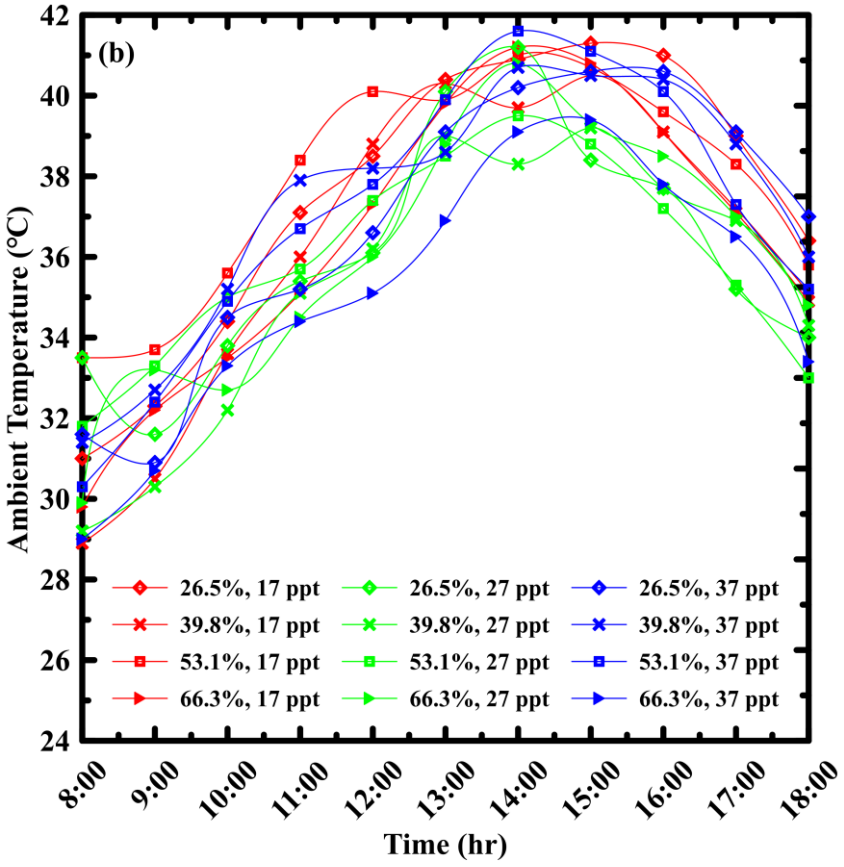
(b)
Ambient Temperature (°C)
42
40
38
36
34
32
30
28
26
24
8:00
9:00
10:00
11:00
12:00
13:00
14:00
15:00
16:00
17:00
18:00
Time (hr)
26.5%, 17 ppt
26.5%, 27 ppt
26.5%, 37 ppt
39.8%, 17 ppt
39.8%, 27 ppt
39.8%, 37 ppt
53.1%, 17 ppt
53.1%, 27 ppt
53.1%, 37 ppt
66.3%, 17 ppt
66.3%, 27 ppt
66.3%, 37 ppt

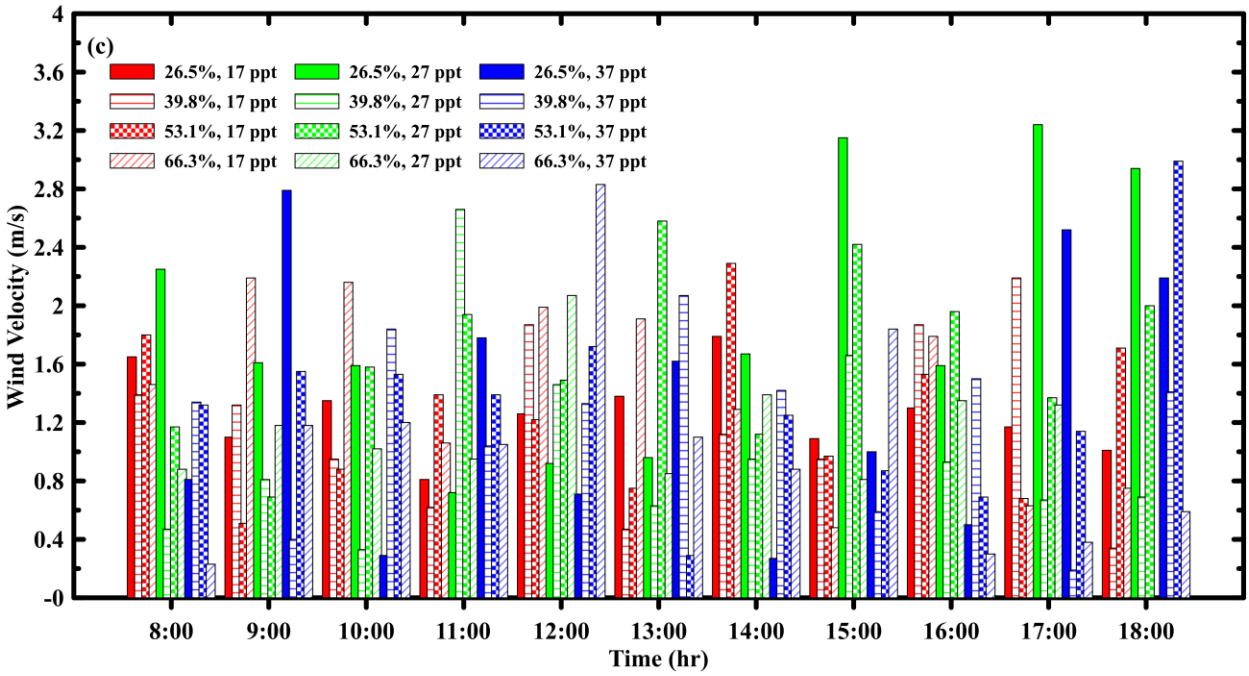

Fig. 5.1 Ambient conditions (a) Direct normal irradiance, (b) ambient temperature, (c) wind velocity.

5.2 Performance Evaluation and Weather Data

The weather data for a typical test day, Wednesday, July 28th, 2022, with specified parameters (filling ratio 53.1%, salinity 17 ppt), is depicted in Fig. 5.2. The ambient air temperature reached its minimum of 33.2 ℃ at 8:15 and progressively rose throughout the experiment, reaching a peak of 42.2 ℃ in the afternoon at 15:15. Wind velocity exhibited notable fluctuations during the experimental period, attaining a maximum of 3.43 m/s at 15:15 and a minimum of 0.18 m/s at 8:30. The highest direct normal irradiance (DNI) recorded was 992.4 W/m^2 at 9:00, while the lowest was 443.6 W/m^2 at sunset (18:00). The average DNI throughout the day was 876.9 W/m^2, with a slight reduction observed between 10:00 and 10:15 due to transient cloud cover.

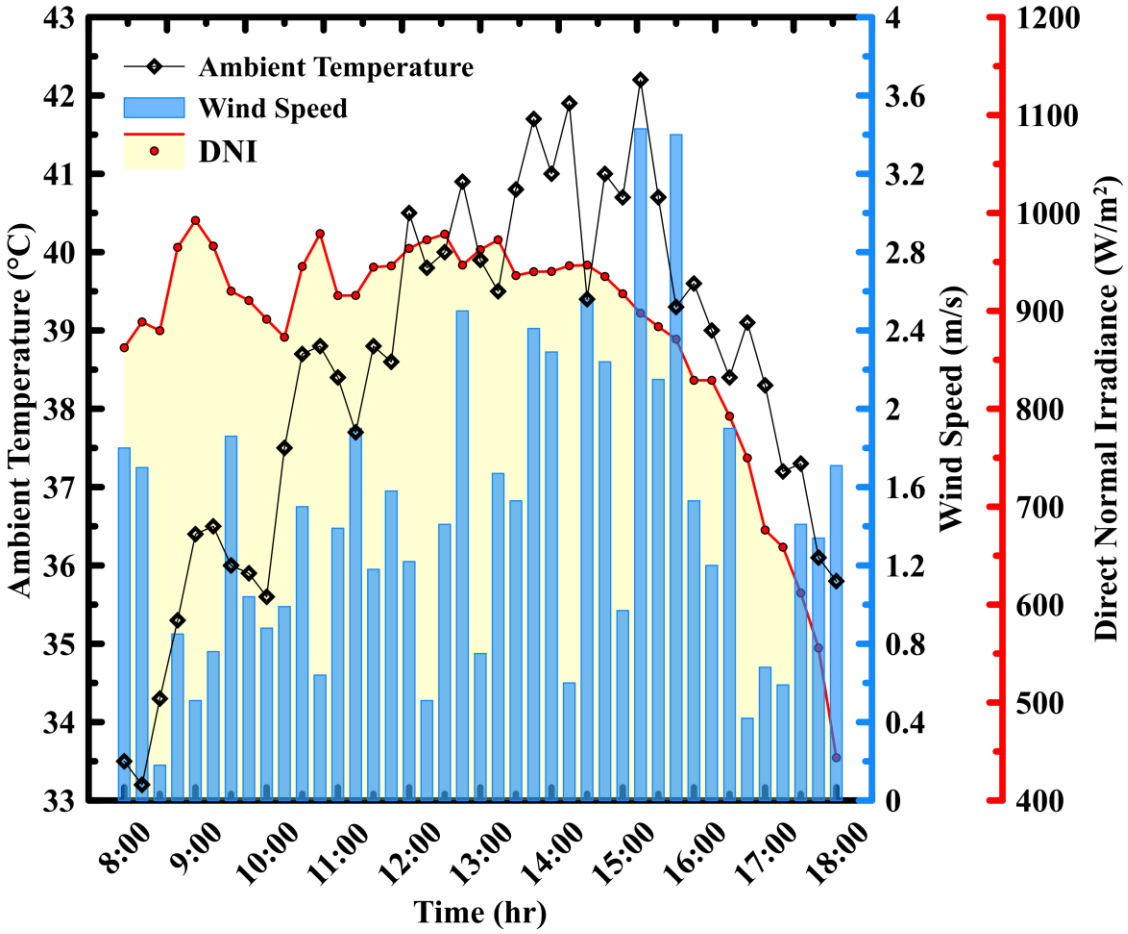

Fig. 5.2 Ambient temperature and wind speed during a typical test (July 28th, 2022).

The hourly fluctuations in the outside and inside temperatures of the absorber plate, as well as the temperatures of the saline water inside the evaporator and the generated vapor, on Wednesday, July 28th, 2022, are illustrated in Fig. 5.3. These measurements were taken with a filling ratio of 53.1% and a feed water salinity of 17 ppt.

At 8:00, the temperatures of the absorber plate outside and inside, the saline water inside the evaporator, and the vapor were recorded as 46.2 ℃, 43.9 ℃, 40.3 ℃, and 38.4 ℃, respectively, as depicted in Fig. 5.3. As observed in the figure, all temperatures exhibit an upward trend during the buildup period until reaching the boiling point at 9:00. At this time, the outside and inside temperatures of the absorber plate were 110.4 ℃ and 107.9 ℃, respectively, while the temperature of the saline

water in the evaporator and the generated vapor were 102.9 ℃ and 100.3 ℃, respectively. The slightly elevated boiling temperature of water can be attributed to the salinity of the water under examination, as evidenced by recent studies.

The system's temperatures exhibit a clear relationship with the DNI, as evidenced by the rapid response observed between 10:00 and 10:15. Notably, this response is primarily governed by DNI and not ambient temperature, given the system's complete insulation except for the small area of the absorber. At 17:30, a slight decline in the outside and inside temperatures of the absorber plate is observed, falling below the temperatures of the saline water and vapor in the solar still. This decline can be attributed to the reduction in DNI. Consequently, the system's productivity during this period is reliant on the stored heat in the solar still.

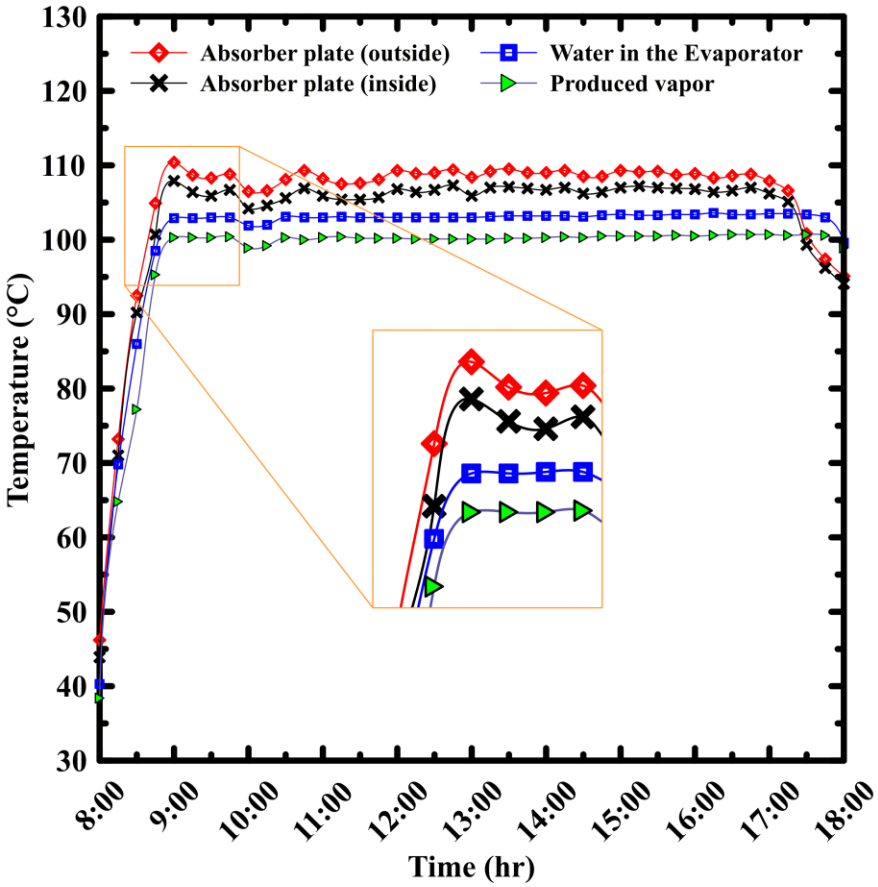

Fig. 5.3 Hourly temperature variation in solar still at a filling ratio of 53.1%, and feed water salinity of 17 ppt (July 28th, 2022).

The solar still's half-hourly distilled water productivity is depicted in Fig. 5.4. Throughout the test period from 8:00 to 18:00, approximately 6 kg/m^2 of distilled water was produced, with the cumulative productivity gradually increasing over time. Initially, the distilled water rate was zero during the first hour due to energy buildup inside the solar still. Subsequently, it reached a peak of 0.941 kg/hr.m^2 at 12:00, coinciding with high ambient temperature and low wind velocity, which minimized thermal losses, as shown in Fig. 5.4. Notably, the effect of the DNI drop on productivity occurred at 10:30, with a slight delay observed between the productivity and the DNI.

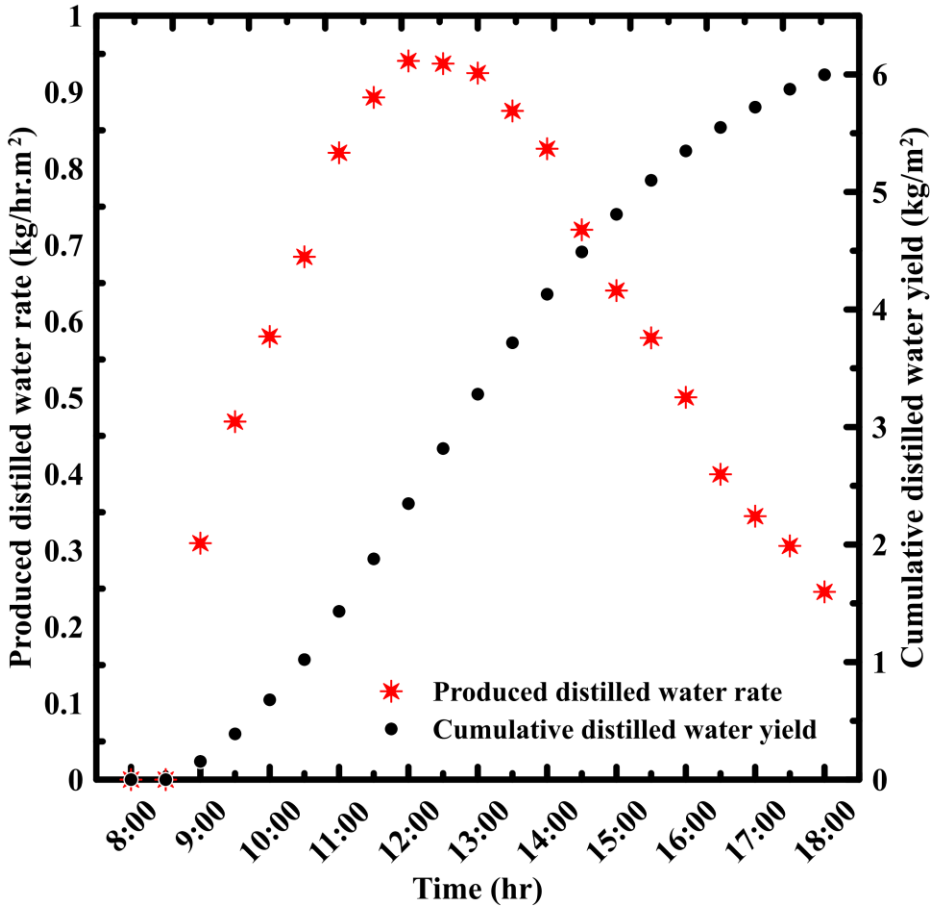

Fig. 5.4 Solar still hourly distilled water productivity fluctuation at a filling ratio of 53.1%, and feed water salinity of 17 ppt (July 28th, 2022).

The incident heat (Q_{solar}), concentrated heat (Q_{conc}), and useful heat (Q_{useful}) are derived from Equations (4.2), (4.3), and (4.11), respectively. The incident heat is influenced by DNI, and mirrors the same trend observed in Fig. 5.5. Additionally, the disparity between the incident heat and concentrated heat curves stems from collector efficiency, impacted by optical properties and geometry, although both curves display similar variations. Lastly, the discrepancy between the concentrated heat and useful heat curves arises from heat losses via radiation (reflection and emission) and convection, computed using Equations (4.5), (4.6), and (4.7), respectively. These losses exhibit continuous fluctuations due to various uncontrollable factors, resulting in significant variability in the useful heat, as depicted in Fig. 5.5.

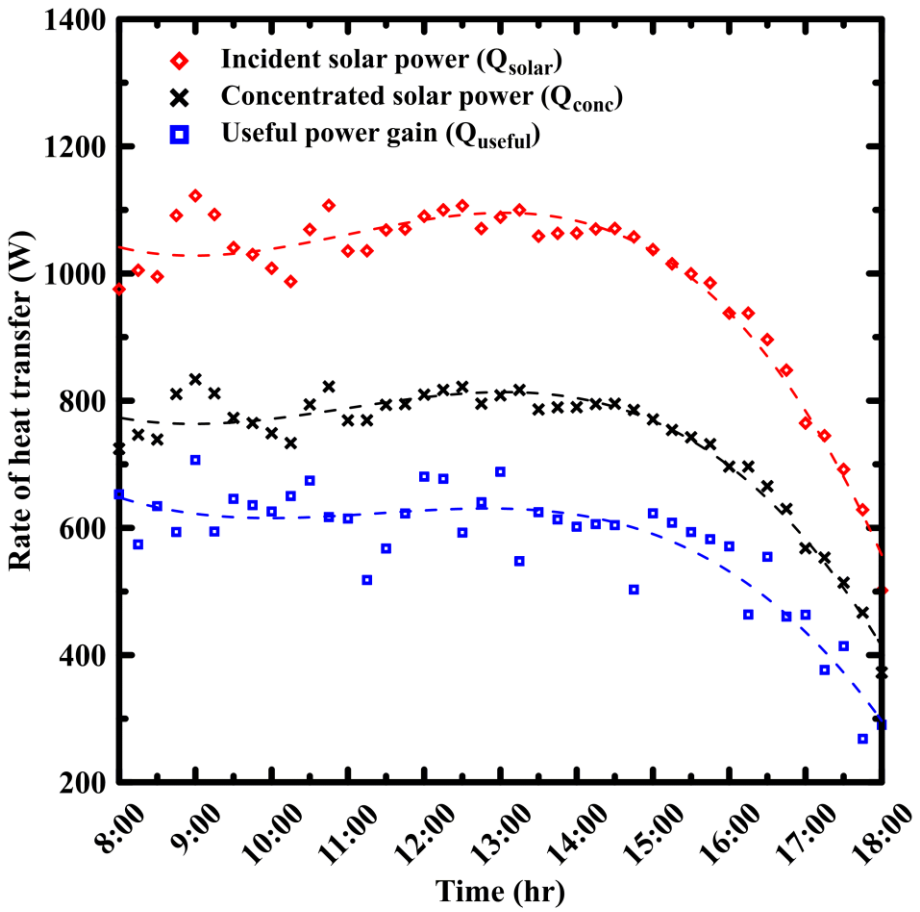

Fig. 5.5 Hourly fluctuation in heat transfer rates in solar still at a filling ratio of 53.1%, and feed water salinity of 17 ppt (July 28th, 2022).

5.3 Effect of Filling Ratio on Solar Still Performance

The solar still filling ratio plays a pivotal role in determining the daily distilled productivity, system efficiency, and overall performance. Increasing the filling ratio of the solar still, from 26.5% to 53.1%, notably enhanced its performance. However, further increasing the filling ratio beyond 53.1% to 66.3% resulted in a decrease in the performance of the solar still.

Initially, the performance enhancement is attributed to two key factors. Firstly, with the increase in the filling ratio, the frequency of the makeup cycle (as described in the experimental procedures section) decreases. This reduction in frequency leads to less energy absorption required for the added water to attain the evaporation temperature. Secondly, the higher filling ratio results in a larger surface area of contact with the absorber plate compared to lower filling ratios. This increased surface area facilitates a more efficient heat transfer coefficient for the system, as illustrated in Fig. 5.6.

Throughout the day, the contact area between water and the absorber plate changes due to sun tracking and frequent variations in elevation angle, as depicted in Fig. 5.7. Additionally, the area of the free water surface, serving as the evaporation surface, remains constant at different filling ratios under the same elevation angle, as shown in Fig. 5.6. Bubbles form on the heating surface of the absorber plate and subsequently rise to the evaporation surface. The longer the distance these bubbles travel, the higher the resistance to the rate of evaporation. This phenomenon becomes more pronounced when the filling ratio reaches 66.3%, which explains the observed drop in the performance of the solar still.

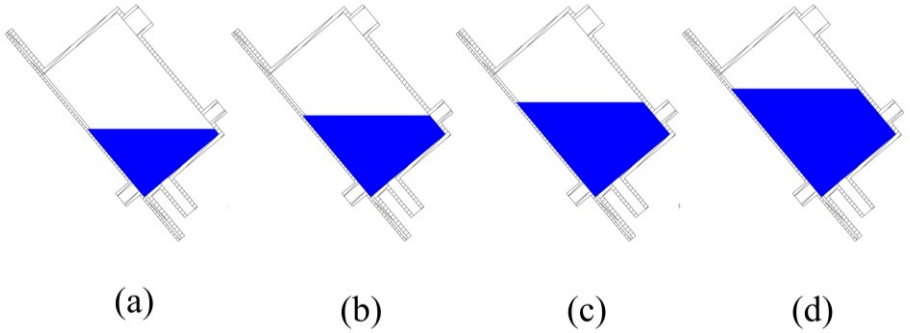

Fig. 5.6 Schematic diagram of solar still at an average elevation angle of 50° with different filling ratios (a) 26.5%, (b) 39.8%, (c) 53.1%, (d) 66.3%.

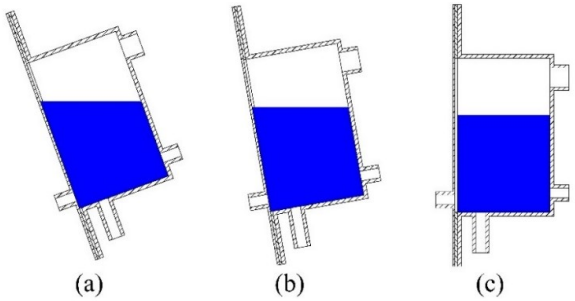

Fig. 5.7 Schematic diagram of solar still at filling ratio 66.3% at various elevation angles (a) 20°, (b) 10°, (c) 0°.

The rate of distilled water for various filling ratios (26.5%, 39.8%, 53.1%, and 66.3%) under different water salinities (17, 27, and 37 ppt) is depicted in Fig. 5.8. The distilled water rate increases with the filling ratio up to 53.1%, before declining at 66.3% for all three salinities. These curves can be segmented into three periods: the first period, from 9:00 to 11:00, exhibits the steepest curves, representing the period of energy buildup; the second period, from 11:30 to 13:30, shows almost flat curves, indicating the utilization of incoming heat energy for evaporation; and the third period, from 14:00 to 18:00, displays less steep downward curves as the DNI gradually decreases while latent heat is retained within the solar still. For a feed water salinity of 17 ppt, the distilled water rates reach their maximum values at 12:00, amounting to 0.829, 0.854, 0.941, and 0.898 kg/hr.m^2 for filling ratios of 26.5%, 39.8%, 53.1%, and 66.3%, respectively.

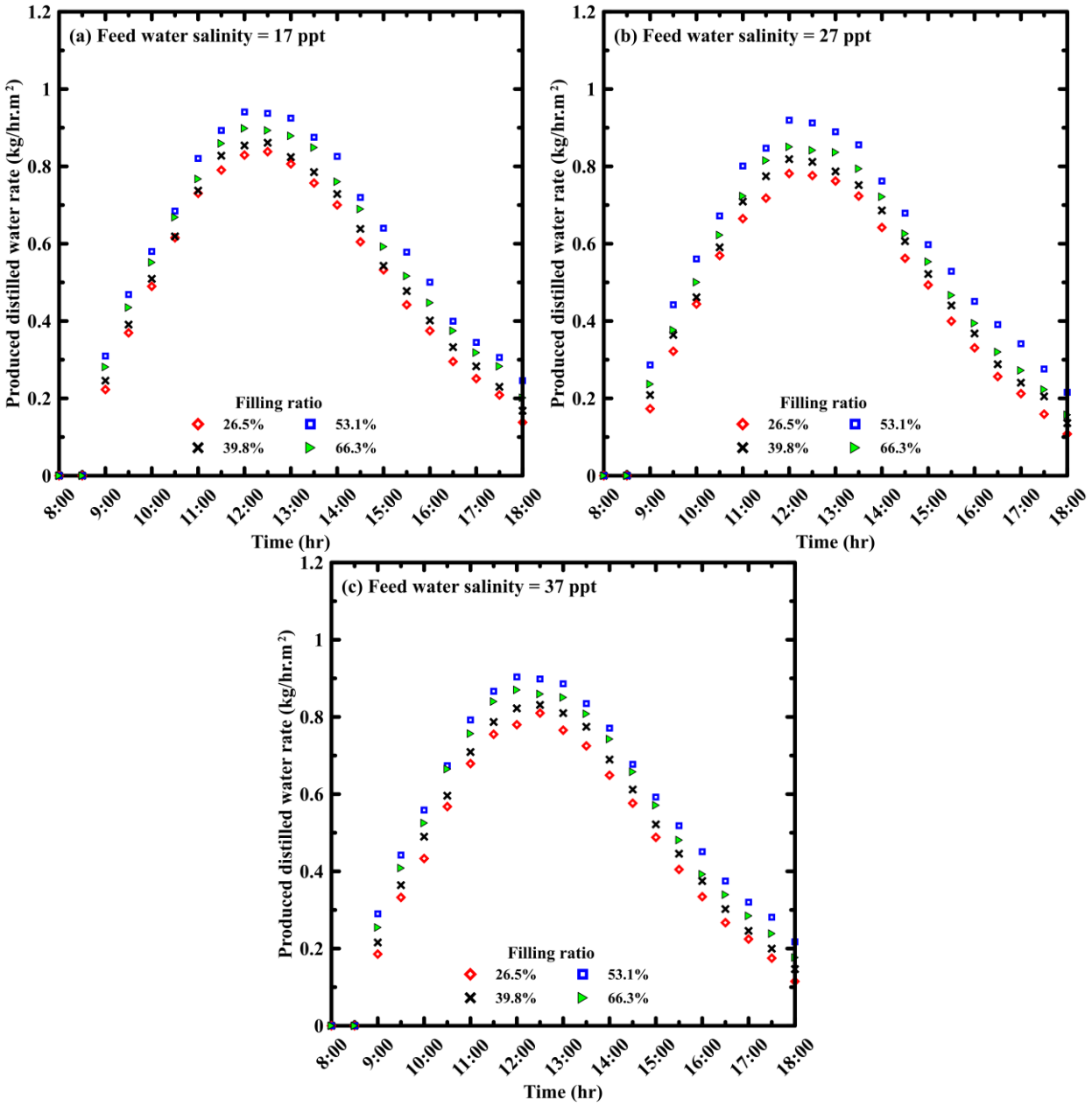

Fig. 5.8 Effect of filling ratio on solar still distilled water rate for different feed water salinities of (a) 17 ppt, (b) 27 ppt, and (c) 37 ppt.

The impact of changing the filling ratio on the system's cumulative productivity is illustrated in Fig. 5.9. Increasing the filling ratio of the still from 26.5% to 53.1% raised the daily cumulative productivity, but it fell at a filling ratio of 66.3%. For a feed water salinity of 17 ppt, the daily cumulative productivity

amounted to 5, 5.23, 6, and 5.63 kg/m^2 for filling ratios of 26.5%, 39.8%, 53.1%, and 66.3%, respectively.

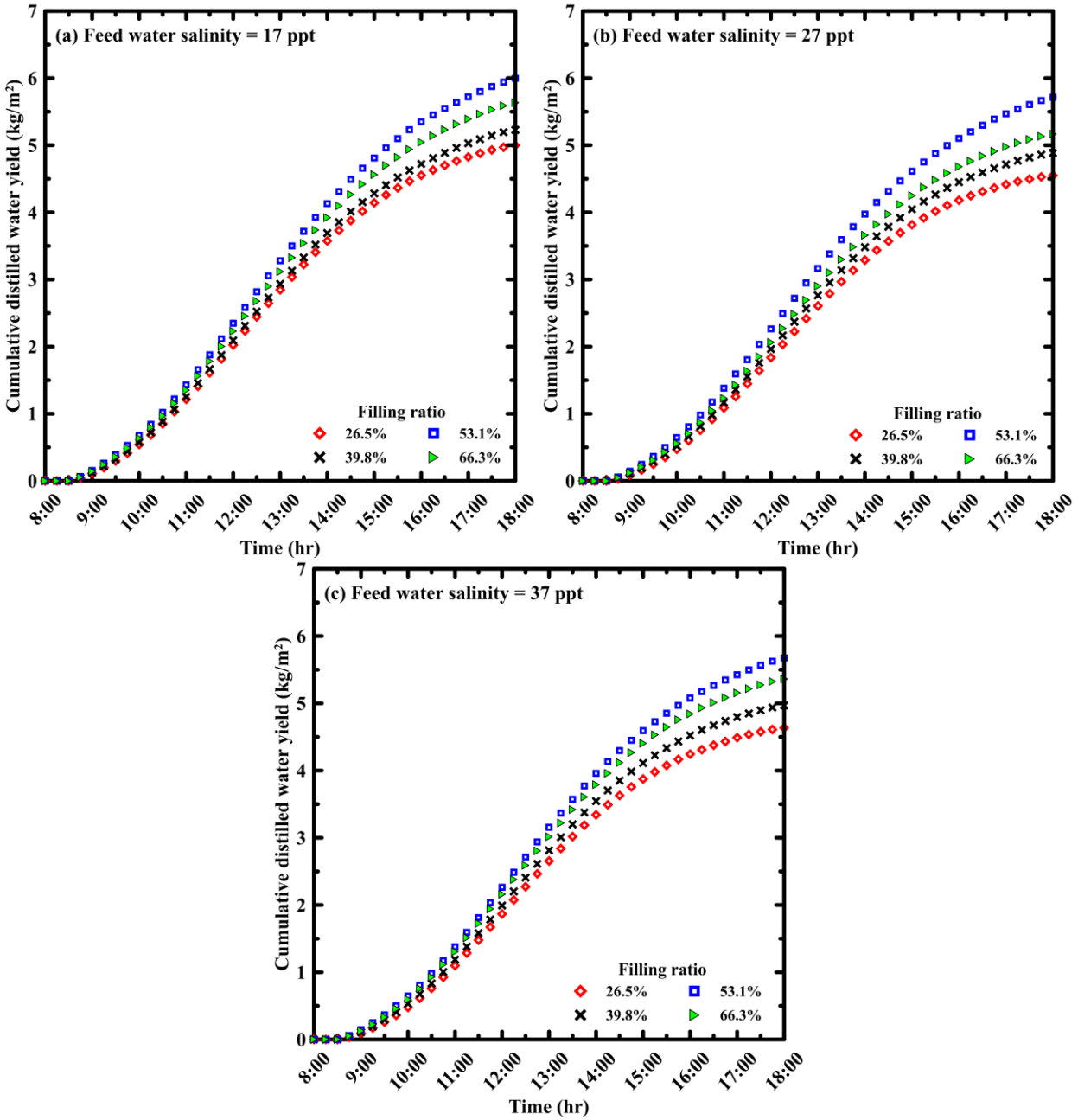

Fig. 5.9 Effect of filling ratio on solar still daily cumulative productivity for different feed water salinities of (a) 17 ppt, (b) 27 ppt, and (c) 37 ppt.

The instantaneous efficiency for different filling ratios, calculated from the hourly distilled water and solar energy using Equation (4.12) is shown in Fig. 5.10. It is evident from the figures that increasing the filling ratio from 26.5% to 53.1% improved the instantaneous efficiency, while further increasing it to 66.3% reduced it. The instantaneous efficiency gradually rises until it peaks between 12:00 and 13:00, coinciding with the maximum distilled water production, after which it gradually declines for the remainder of the test hours.

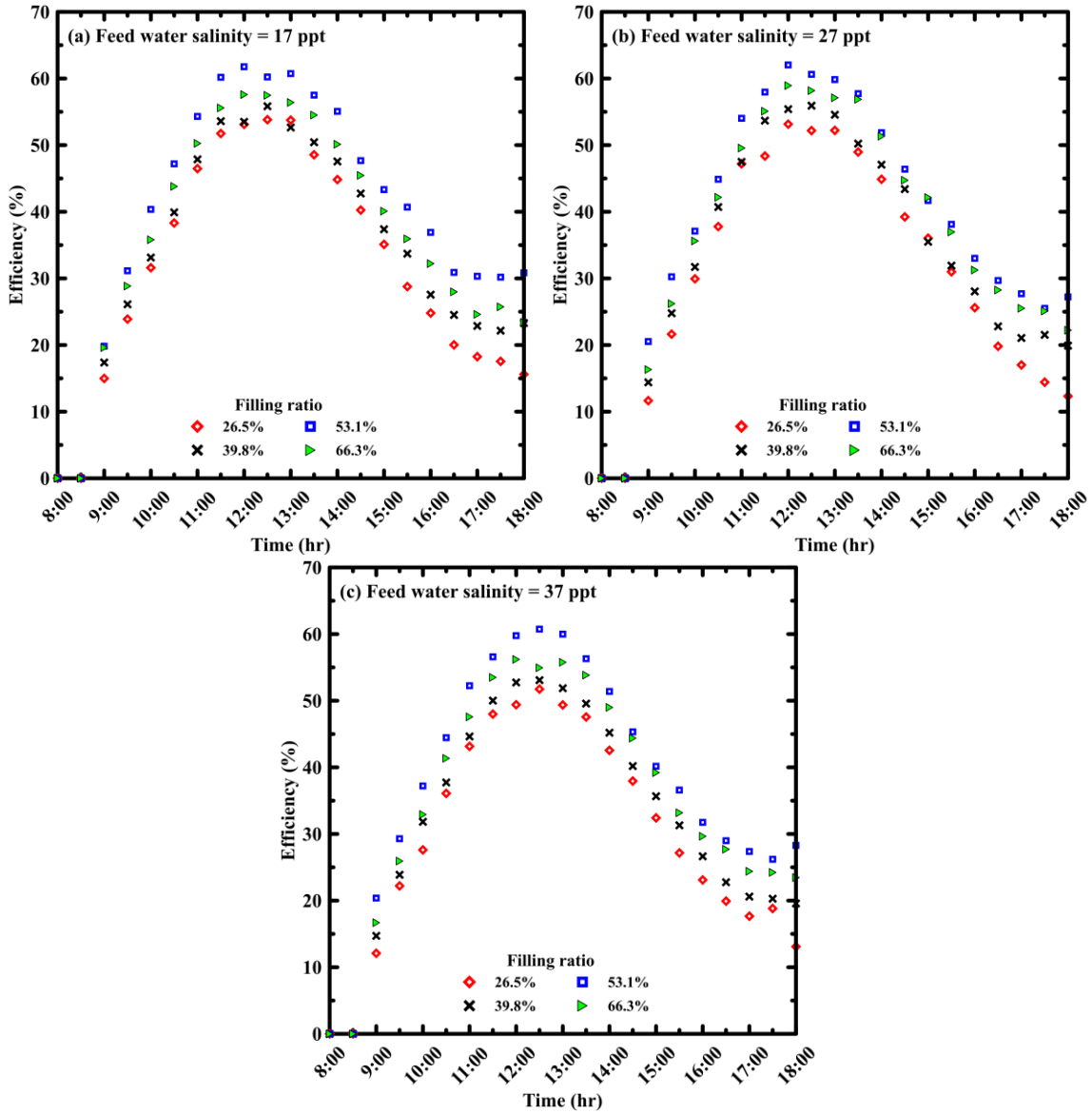

Fig. 5.10 Effect of filling ratio on instantaneous efficiency for different feed water salinities of (a) 17 ppt, (b) 27 ppt, and (c) 37 ppt.

However, during the final period from 17:00 to 18:00, the instantaneous efficiency either remains constant or slightly increases, as the DNI decreases, and the production of vapor and distilled water continues based on the stored heat energy inside the solar still. At 12:00, for a feed water salinity of 17 ppt, the instantaneous efficiencies were 53.11%, 54.31%, 61.77%, and 57.59% for filling ratios of 26.5%, 39.8%, 53.1%, and 66.3%, respectively.

5.4 Effect of Varying Feed Water Salinity

The effect of salinity, within the range of 17 to 37 ppt with increment of 10 ppt, was comprehensively analyzed to assess its influence on the performance of the desalination system. The results indicated that both distilled water productivity and overall system efficiency exhibited only slight reductions as salinity levels increased. This minimal impact is a favorable outcome for the proposed desalination system, as it confirms its ability to effectively desalinate a wide range of water sources, from brackish and saline water to highly saline and even brine water. However, it is important to note that higher salinity levels result in an increase in the boiling point, thereby requiring more energy to evaporate the saline water. Moreover, as the feed water's salinity rises, there is a gradual accumulation of precipitated salts on the wall of the absorber plate. Over time, this salt buildup acts as an insulating layer, reducing heat transfer efficiency and subsequently limiting the performance of the solar still.

A comprehensive comparison of the distilled water production rates for different feed water salinity levels, specifically ranging from 17 to 37 ppt is depicted in Fig. 5.11. The analysis shows that the maximum rate of distilled water was obtained at the lowest salinity of 17 ppt. In contrast, the distilled water production rates for salinities of 27 and 37 ppt were remarkably close to one another. This

similarity can be attributed to variations in solar irradiance, particularly the lower average solar irradiance encountered during the experiments conducted with the 27 ppt sample, which likely influenced the overall water production.

As discussed earlier, the pattern of distilled water generation can be distinctly categorized into three key phases throughout the day. The first phase, identified as the energy buildup phase, extends from 9:00 to 11:00, during which the system accumulates energy and begins heating the saline water. Following this is the second phase, which occurs between 11:30 and 13:30, representing the period of peak evaporation. During this interval, the most significant quantity of water is evaporated due to the high solar irradiance and optimized energy absorption. The final phase, from 14:00 to 18:00, marks a decline in distilled water production as the available solar energy decreases and evaporation rates slow down.

At 12:30, when the filling ratio was set at 26.5%, the system's performance was observed to vary across different salinity levels. For feed water salinities of 17, 27, and 37 ppt, the corresponding distilled water production rates were 0.838, 0.777, and 0.81 kg/hr.m^2, respectively. This finding underscores the system's ability to maintain relatively consistent performance, even at higher salinity levels, and highlights the influence of solar irradiance and salinity on the desalination process.

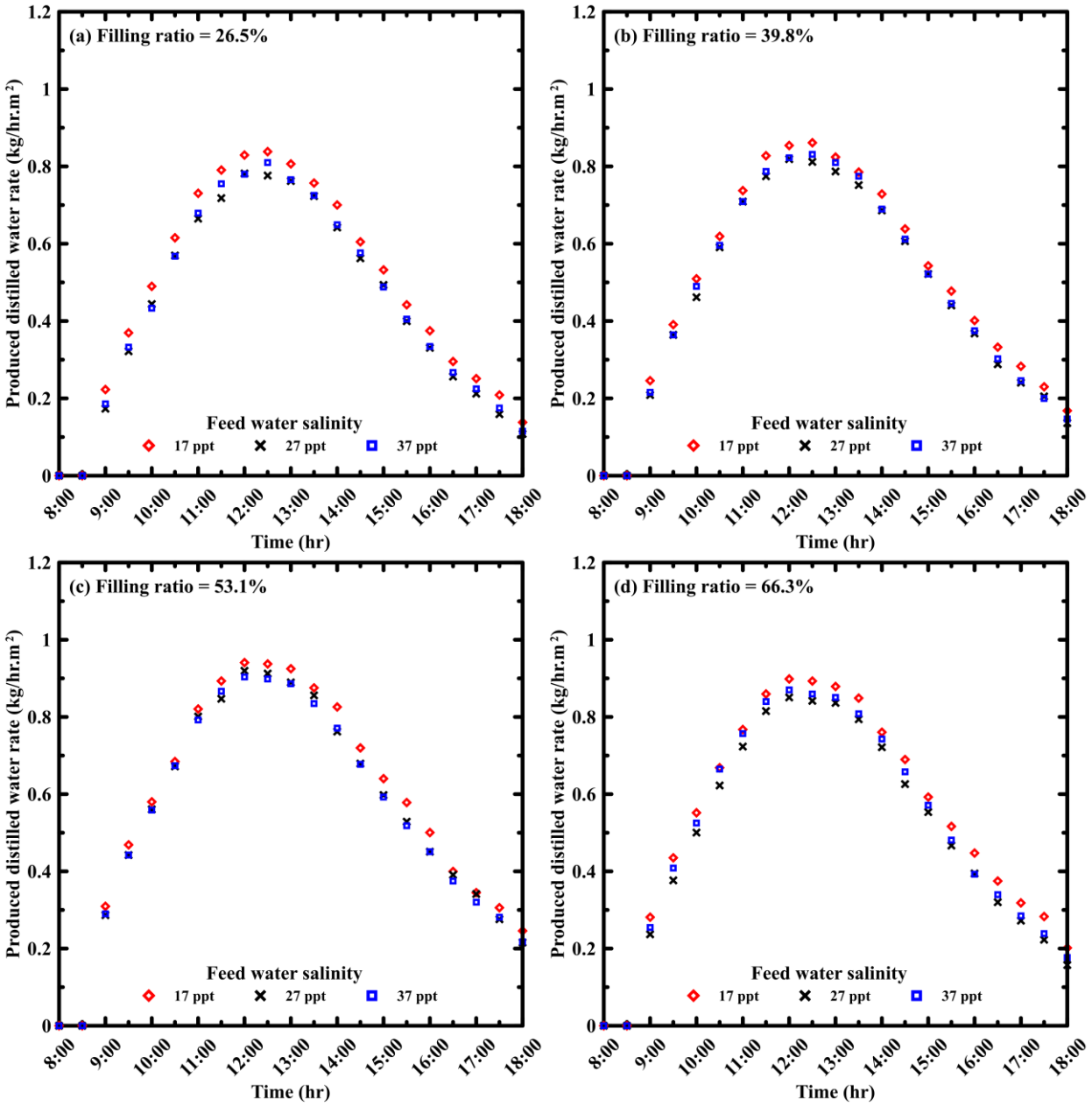

Fig. 5.11 Effect of feed water salinity on solar still distilled water rate for different filling ratios of (a) 26.5%, (b) 39.8%, (c) 53.1%, (d) 66.3%.

The impact of feed water salinity on the cumulative productivity of the system is illustrated in Fig. 5.12. It is observed that increasing the feed water salinity results in a reduction in cumulative productivity. Specifically, elevating the feed water salinity from 17 ppt to 27 and 37 ppt resulted in a decrease in cumulative productivity from 6 kg/m^2 to 5.72 and 5.68 kg/m^2, respectively, at a filling ratio of 53.1%.

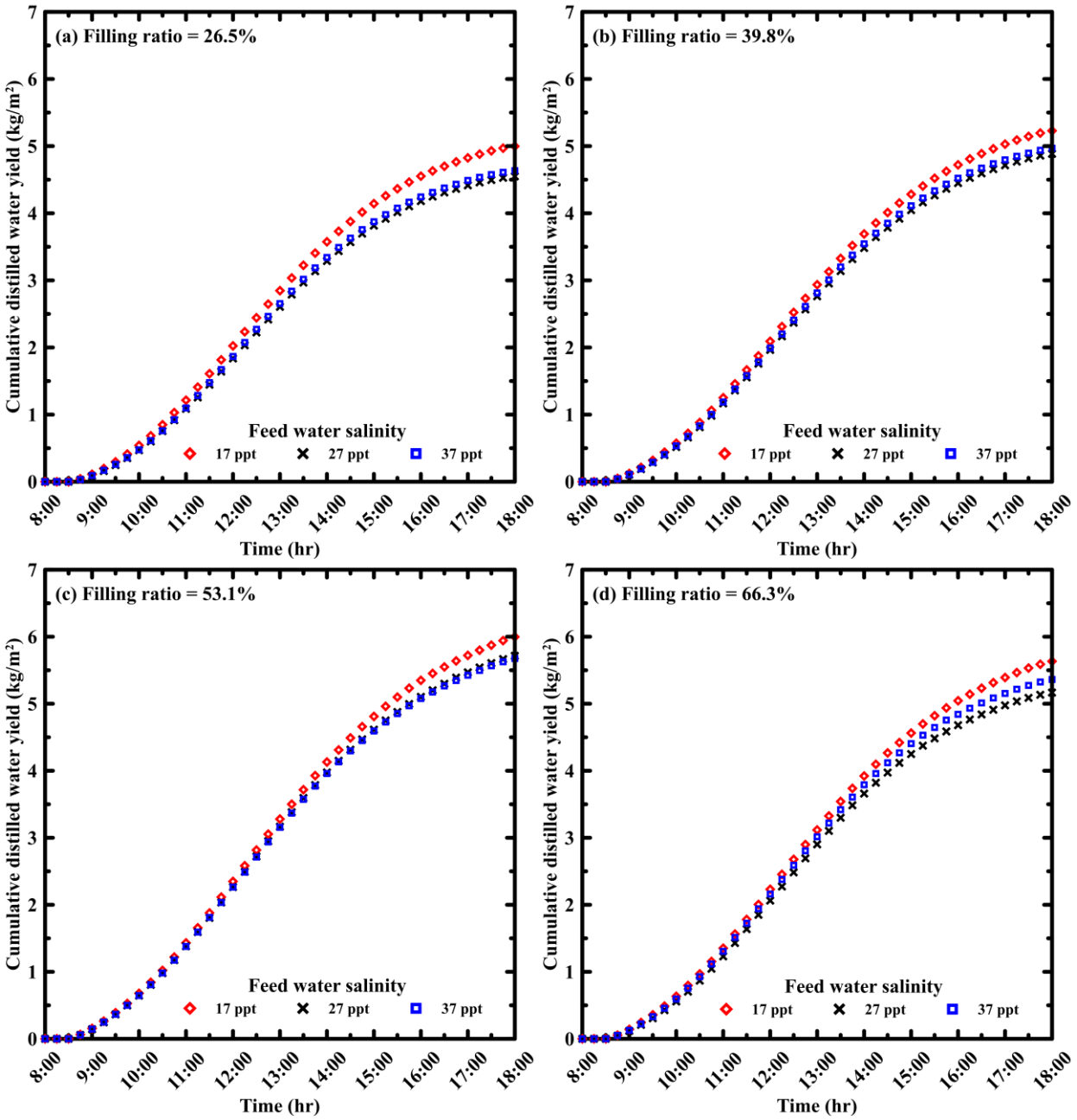

Fig. 5.12 Effect of feed water salinity on solar still daily cumulative productivity for different filling ratios of (a) 26.5%, (b) 39.8%, (c) 53.1%, (d) 66.3%.

The instantaneous efficiency calculated from Equation (4.12) for various feed water salinities is depicted in Fig. 5.13. It is observed that the instantaneous efficiency remains relatively similar with minor differences, but it decreases insignificantly with increasing feed water salinity. Notably, the efficiency exhibits a

consistent or slightly increasing trend during the period of 17:00 to 18:00, attributed to the decrease in DNI and vapor generation, which relies on stored energy (as discussed in the previous section). At 12:00, the maximum instantaneous efficiency values for a filling ratio of 53.1% are 61.77%, 62.03%, and 59.77% for feed water salinities of 17, 27, and 37 ppt, respectively.

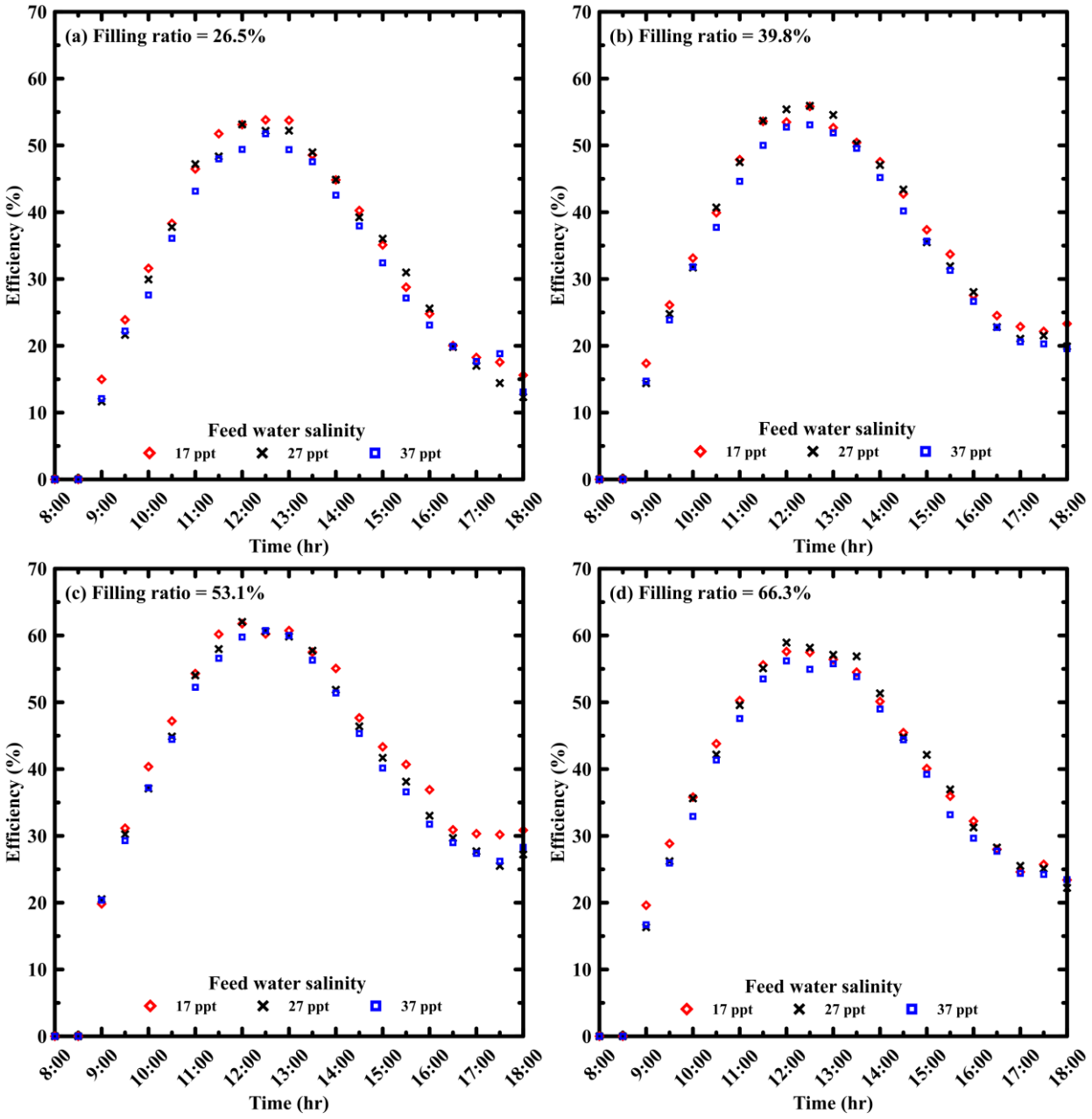

Fig. 5.13 Effect of feed water salinity on instantaneous efficiency for different filling ratios of (a) 26.5%, (b) 39.8%, (c) 53.1%, (d) 66.3%.

A comprehensive overview of the daily cumulative productivity and system efficiency of the proposed system across various investigated operating parameters is provided in Fig. 5.14. It is evident that increasing the filling ratio from 26.5% to 53.1% results in an average enhancement of daily productivity and system efficiency by 22.7% and 26.3%, respectively. However, a further increase in the filling ratio from 53.1% to 66.3% leads to an average decrease in daily productivity and system efficiency by 7.1% and 6.9%, respectively.

Conversely, elevating the feed water salinity causes a reduction in both daily cumulative productivity and system efficiency. Specifically, when the feed water salinity is raised from 17 ppt to 27 ppt, the values of daily productivity and system efficiency decrease by 7.1% and 2.2%, respectively. Similarly, increasing the feed water salinity from 17 ppt to 37 ppt results in reductions of 5.6% and 5.1% in daily productivity and system efficiency, respectively. These trends should be considered alongside the lower average solar irradiance during the experiments conducted using the 27 ppt sample.

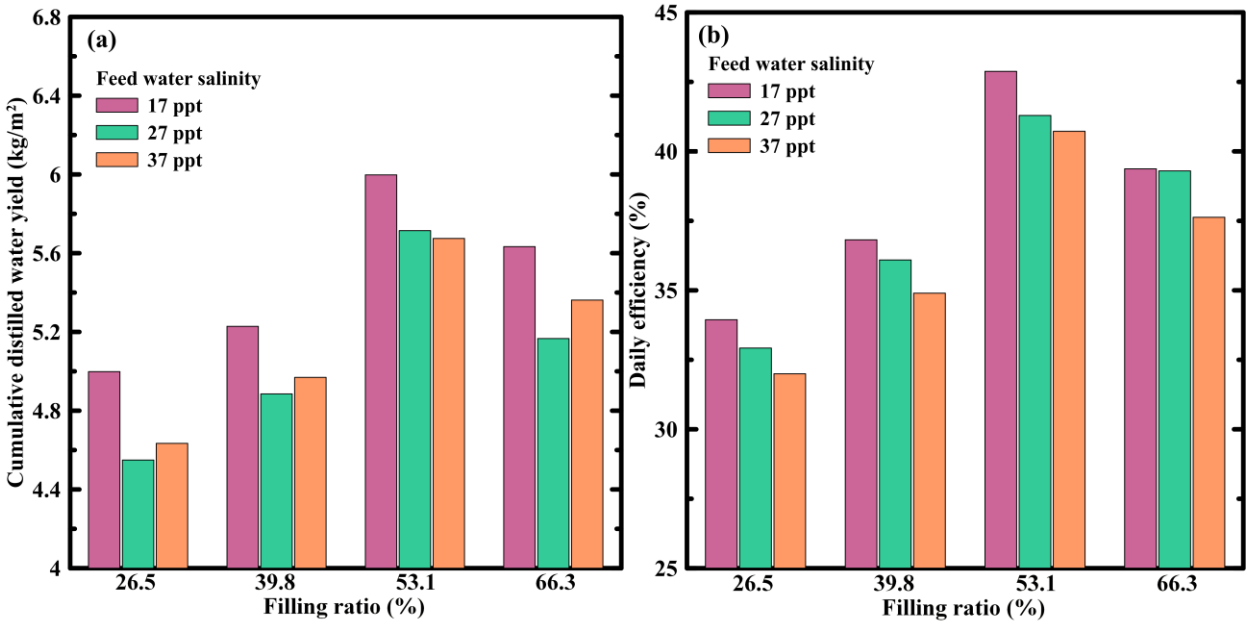

Fig. 5.14 Effect of feed water salinity and filling ratio on solar still (a) cumulative productivity (b) daily system efficiency.

5.5 Economic Analysis

In addition to considerations such as design simplicity, ease of implementation, and component availability, the foremost objective behind the development of a novel solar desalination unit is to provide access to clean freshwater at an affordable cost, thereby addressing the needs of rural and isolated communities.

For a thorough assessment of the system's economic feasibility over a year, the annual productivity is determined by multiplying the average production during the summer months by the average number of sunny days in the region where testing occurs. Sunny days annually typically range from 250 to 340 in different countries [22], [31]-[36], [39], [40], [44], [55]-[58], with Egypt falling within this range at 300 to 340 days [40], [44], [57]. For this study, the average value within Egypt's specified range is utilized. This daily average distilled productivity serves as a crucial benchmark for evaluating the overall performance and efficiency of the system. Additionally, it highlights the importance of extending the analysis beyond the summer season to capture variations in climatic conditions throughout the year. While the current data reflects operational outcomes during hot summer conditions, it is essential to examine the system's performance during contrasting winter conditions.

Table 5.1 displays the cost estimation for the main components of the proposed system. The total fixed cost of the system amounts to approximately 231.6$. The average cost of distilled water is determined using the Equation (5.1):

$$C = F + V = F + (0.3 \times F \times n) \tag{5.1}$$

Where n is the expected solar still lifespan, V is the variable cost, and C is the total cost.

Table 5.1 Cost estimation of the solar still component.

Item	**Price ($)**
Iron sheet	29.7
SDC	44.7
Mirror	6.4
Tracking system	75.6
Pump	29.4
Connections and Fittings	45.8
Total	231.6

For a projected lifespan of 10 years for this proposed unit and an estimated variable cost of 30% of the fixed cost per year, as employed in previous studies [40], [57], the total cost (C) is calculated as follows:

$C = 231.6 + (0.3 \times 231.6 \times 10) = 926.4\ \$$

Based on the experimental findings, the daily average distilled productivity of the system is determined to be 5.92 kg/day. Assuming the distillation system operates for approximately 320 days per year, considering the consistent sunlight throughout the year in Egypt, the total distilled yield over the system's lifespan is $5.92 \times 10 \times 320 = 18944$ kg.

Therefore, the cost of producing one kilogram of freshwater is calculated as:

$\mathrm{CPL} = 926.4/18944 = 0.0489\ \$$

Table 5.2 provides a detailed comparison between the findings of the current study and those from prior investigations involving both conventional solar stills and solar stills integrated with solar dish concentrators. In the present study, the daily cumulative productivity was recorded at 6 kg/m², placing it within the productivity range reported in previous studies on concentrated solar stills, which have been shown to produce between 4.44 and 6.5 kg/m². This performance not only falls within the upper limits of what has been achieved with concentrated solar stills but also significantly surpasses the productivity of conventional solar stills, which have

demonstrated lower daily outputs ranging from 1.19 to 4.235 kg/m². The findings highlight the enhanced efficiency and productivity of systems employing solar dish concentrators over traditional solar stills, reinforcing the benefits of incorporating concentrators in solar desalination processes. This improvement is clearly illustrated in Fig. 5.15.

The increased efficiency of the solar still system can be attributed to the concentration of solar radiation on the absorber plate, resulting in elevated water temperatures and reaching the boiling point, thereby enhancing the generation of vapor. The system efficiency of the proposed system exceeded that of conventional solar stills (ranging from 11% to 31.46%). Moreover, when compared to concentrated solar stills, the efficiency of the proposed system was higher than that reported by Tawfik [44].

The influence of the concentration ratio (CR) on the cost of distilled water becomes evident through a comparative analysis of various systems. For instance, Tawfik's system [44], which operates with a lower concentration ratio than the system proposed in this study, resulted in a comparatively higher CPL, indicating less cost-effectiveness. On the other hand, Omara's system [40], with a concentration ratio exceeding that of the proposed system, demonstrated a notably lower CPL, underscoring the advantages of a higher CR in reducing water production costs. This contrast highlights the critical role that the concentration ratio plays in enhancing water production efficiency and lowering operational costs. Additionally, when comparing these systems to the global average CPL for water production, which stands at $0.474 [59], the results of the current study are particularly notable, showcasing a significantly competitive and efficient CPL. This reinforces the effectiveness of the proposed system in producing distilled water at a lower cost,

making it a promising alternative for large-scale applications in regions facing water scarcity.

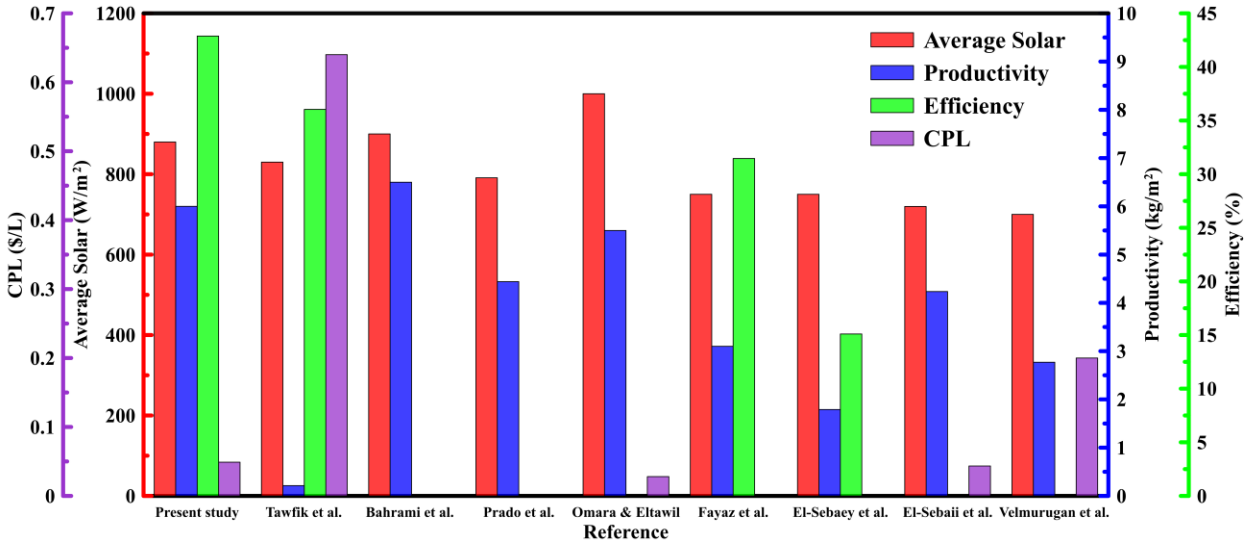

Fig. 5.15 Comparison between different results for solar still coupled with SDC and CSS.

Table 5.2 Comparison between different results for solar still coupled with SDC and CSS.

	Solar still with dish concentrator					Conventional solar still			
	Present	Tawfik et al. [44]	Bahrami et al. [41]	Prado et al. [38]	Omara & Eltawil [40]	Fayaz et al. [62]	El-Sebaey et al. [16]	El-Sebaii et al. [61]	Velmurugan et al. [60]
Year	2022	2020	2019	2015	2012	2021	2018	2014	2006-2007
Study Type	Experimental	Experimental -Theoretical	Theoretical	Theoretical	Experimental	Experimental	Experimental	Experimental -Theoretical	Experimental
Location	30.07º N 31.24º E	30.57° N 31.50° E	30.66° N 51.58° E	18.91° S 48.25 °W	31.07 °N 30.57 °E	30.77 °N 76.57 °E	30.5 °N 31.01 °E	30.79 °N 31 °E	9.93 °N 78.12 °E
Avg. Solar (W/m^2)	824.2–923.2	818.4–842.3	850–900	791	1000	750	750	719.7	700
Concentration Ratio	12.5	4.23[a]	78.55a	133.3a	17.2a	1	1	1	1
Yield (kg/m^2)	6[b]	0.213[c]	5.7 – 6.5	4.44d	5.5	3.1	1.19 –1.79	4.235	2.77
Efficiency (%)	42.88[b]	36.04[c]	-	-	-	31.46	11 – 15.1	-	-
CPL ($/L)	0.0489	0.64	-	-	0.028	-	-	0.0434	0.2

[a] Calculated based on data.
[b] At 17 ppt salinity and 53.1% filling ratio of solar still.
[c] At 15 ppt salinity and 0.75 kg of saline water mass in solar still.
[d] At 20 ppt salinity and 100 mL of saline water mass in solar still.

CHAPTER 6

CONCLUSION AND FUTURE WORK RECOMMENDATION

6.1 Introduction

The present study investigates the experimental performance of an innovative sun-tracking concentrated solar still under Egyptian weather conditions. The solar still comprises a cylindrical stainless steel structure with a copper absorber plate, strategically positioned at the focal point of an SDC covered with reflective mirrors to concentrate solar radiations, resulting in a solar concentration ratio of 12.5.

The primary objective is to explore novel approaches for supplying freshwater to rural areas in a manner that is both straightforward and cost-effective. Throughout the summer of 2022, the system's performance was evaluated by varying two key parameters. At first the salinity of the feed water 17 ppt, 27 ppt, 37 ppt, mimicking the conditions of seawater in the Mediterranean Sea and two types of brackish water in Egypt. Secondly the filling ratio of the solar still. Four filling ratios were examined 26.5%, 39.8%, 53.1%, and 66.3%, corresponding to saline water masses of 1 kg, 1.5 kg, 2 kg, and 2.5 kg, respectively.

6.2 Conclusion

The key conclusions drawn from the current study are summarized as follows:

- Increasing the filling ratio from 26.5% to 53.1% enhanced daily cumulative productivity by 22.69% and system efficiency by 26.34%. However, when the filling ratio was further increased from 53.1% to

66.3%, productivity and efficiency decreased by approximately 7.06% and 6.87%, respectively.

- The rise of feed water salinity from 17 ppt to 37 ppt resulted in a reduction of approximately 5.61% in daily cumulative productivity and a decrease of 5.1% in daily system efficiency.
- The optimal operational parameters for the solar still system are a filling ratio of 53.1% and a salinity level of 17 ppt, which result in a daily cumulative productivity of 6 kg/m² and a system efficiency of 42.88%.
- The economic analysis indicated favorable feasibility, with the cost of desalinated water estimated at $0.0489 per liter, demonstrating competitive pricing relative to other solar desalination technologies.

6.3 Future Work Recommendation

The current study identifies several areas for potential improvement, and suggests the following avenues for further research:

- Assess the system's performance under varying climatic conditions throughout the year, especially in cloudy weather, to better understand its capabilities.
- Explore the integration of photovoltaic cells to power the system, enhancing its sustainability and enabling its use in rural areas lacking grid connectivity or access to external energy sources.

References

[1] "Earth's Water Resources - ASLO." Accessed: Mar. 27, 2024. [Online]. Available: https://www.aslo.org/what-is-aquatic-science/earths-water-resources/

[2] D. Curto, V. Franzitta, and A. Guercio, "A review of the water desalination technologies," Jan. 02, 2021, *MDPI AG*. doi: 10.3390/app11020670.

[3] M. R. Qtaishat and F. Banat, "Desalination by solar powered membrane distillation systems," *Desalination*, V. 308, pp. 186–197, Jan. 2013, doi: 10.1016/j.desal.2012.01.021.

[4] "Renewable Energy | Department of Energy." Accessed: Mar. 29, 2023. [Online]. Available: https://www.energy.gov/eere/renewable-energy

[5] "Global Solar Atlas." Accessed: Mar. 29, 2023. [Online]. Available: https://globalsolaratlas.info/download/egypt

[6] D. Sakthivadivel, K. Balaji, D. Dsilva Winfred Rufuss, S. Iniyan, and L. Suganthi, "Solar energy technologies: principles and applications," in *Renewable-Energy-Driven Future: Technologies, Modelling, Applications, Sustainability and Policies*, Elsevier Applied Science, 2020, pp. 3–42. doi: 10.1016/B978-0-12-820539-6.00001-7.

[7] O. Bait, "Direct and indirect solar–powered desalination processes loaded with nanoparticles: A review," *Sustainable Energy Technologies and Assessments*, V. 37, Feb. 2020, doi: 10.1016/j.seta.2019.100597.

[8] J. E. Miller, "Review of water resources and desalination techniques," no. May, 2003, doi: 10.2172/809106.

[9] M. Shatat and S. B. Riffat, “Water desalination technologies utilizing conventional and renewable energy sources,” *International Journal of Low-Carbon Technologies*, V. 9, no. 1, pp. 1–19, Mar. 2014, doi: 10.1093/ijlct/cts025.

[10] I. Sarbu and C. Sebarchievici, “Solar Collectors,” in *Solar Heating and Cooling Systems*, Elsevier, 2017, pp. 29–97. doi: 10.1016/B978-0-12-811662-3.00003-7.

[11] S. A. Kalogirou, *Solar thermal collectors and applications*, V. 30, no. 3. 2004. doi: 10.1016/j.pecs.2004.02.001.

[12] O. Aliman, I. Daut, and R. Adzman, “Simplification of Sun Tracking Mode to Gain High Concentration Solar Energy,” *Am J Appl Sci*, V. 4, no. 3, pp. 171–175, 2007.

[13] A. Jamar, Z. A. A. Majid, W. H. Azmi, M. Norhafana, and A. A. Razak, “A review of water heating system for solar energy applications,” *International Communications in Heat and Mass Transfer*, V. 76, pp. 178–187, Aug. 2016, doi: 10.1016/J.ICHEATMASSTRANSFER.2016.05.028.

[14] Y. Tian and C. Y. Zhao, “A review of solar collectors and thermal energy storage in solar thermal applications,” *Appl Energy*, V. 104, pp. 538–553, Apr. 2013, doi: 10.1016/J.APENERGY.2012.11.051.

[15] M. I. Al-Amayreh, A. Alahmer, and A. Manasrah, “A novel parabolic solar dish design for a hybrid solar lighting-thermal applications,” *Energy Reports*, V. 6, pp. 1136–1143, Dec. 2020, doi: 10.1016/J.EGYR.2020.11.063.

[16] M. S. El-Sebaey, A. Ellman, A. Hegazy, and H. Panchal, “Experimental study and mathematical model development for the effect of water depth on water

production of a modified basin solar still," *Case Studies in Thermal Engineering*, V. 33, May 2022, doi: 10.1016/j.csite.2022.101925.

[17] A. Muthu Manokar Y. Taamneh, A.E. Kabeel, D. Prince Winston, P. Vijayabalan, D. Balaji, R. Sathyamurthy, S. Padmanaba Sundar, D. Mageshbabu, "Effect of water depth and insulation on the productivity of an acrylic pyramid solar still – An experimental study," *Groundw Sustain Dev*, V. 10, Apr. 2020, doi: 10.1016/j.gsd.2019.100319.

[18] T. Maridurai, S. Rajkumar, M. Arunkumar, V. Mohanavel, K. Arul, D. Madhesh, Ram Subbiah, "Performance study on phase change material integrated solar still coupled with solar collector," *Mater Today Proc*, V. 59, pp. 1319–1323, Jan. 2022, doi: 10.1016/j.matpr.2021.11.539.

[19] H. Panchal, Kishor Kumar Sadasivuni, Alim Al Ayub Ahmed, Sanil S Hishan, Mohammad Hossein Doranehgard, Fadl Abdelmonem Essa, S. Shanmugan, Mohammad khalid, "Graphite powder mixed with black paint on the absorber plate of the solar still to enhance yield: An experimental investigation," *Desalination*, V. 520, no. September, p. 115349, 2021, doi: 10.1016/j.desal.2021.115349.

[20] A. Rahmani, F. Khemmar, and Z. Saadi, "Experimental investigation on the negative effect of the external condenser on the conventional solar still performance," *Desalination*, V. 501, no. August 2020, p. 114914, 2021, doi: 10.1016/j.desal.2020.114914.

[21] V. K. Thakur and M. K. Gaur, "Study the effect of CuO nanoparticles on the performance of passive solar still in winter and summer season," *Mater Today Proc*, V. 57, pp. 2009–2017, Jan. 2022, doi: 10.1016/j.matpr.2021.11.119.

[22] R. Dhivagar, S. Shoeibi, S. M. Parsa, S. Hoseinzadeh, H. Kargarsharifabad, and M. Khiadani, “Performance evaluation of solar still using energy storage biomaterial with porous surface: An experimental study and environmental analysis,” *Renew Energy*, V. 206, no. December 2022, pp. 879–889, 2023, doi: 10.1016/j.renene.2023.02.097.

[23] A. A. Alshqirate, A. S. Awad, A. Al Alawin, and M. A. Essa, “Experimental investigation of solar still productivity enhancement of distilled water by using natural fibers,” *Desalination*, V. 553, no. October 2022, p. 116487, 2023, doi: 10.1016/j.desal.2023.116487.

[24] R. Shah, M. Makwana, N. Makwana, and R. Desai, “Perfromance analysis of black gravel solar still,” *Mater Today Proc*, V. 72, pp. 1000–1006, Jan. 2023, doi: 10.1016/j.matpr.2022.09.115.

[25] S. Tiwari and P. K. S. Rathore, “Performance enhancement of solar still for water desalination integrated with thermal energy storage,” *Mater Today Proc*, V. 74, pp. 202–206, Jan. 2023, doi: 10.1016/j.matpr.2022.08.048.

[26] M. Jahanpanah, S. J. Sadatinejad, A. Kasaeian, M. H. Jahangir, and H. Sarrafha, “Experimental investigation of the effects of low-temperature phase change material on single-slope solar still,” *Desalination*, V. 499, no. November 2020, p. 114799, 2021, doi: 10.1016/j.desal.2020.114799.

[27] M. Al-Harahsheh, M. Abu-Arabi, M. Ahmad, and H. Mousa, “Self-powered solar desalination using solar still enhanced by external solar collector and phase change material,” *Appl Therm Eng*, V. 206, no. January, p. 118118, 2022, doi: 10.1016/j.applthermaleng.2022.118118.

[28] S. W. Sharshir, M. A. Rozza, M. Elsharkawy, M. M. Youns, F. Abou-Taleb, and A. E. Kabeel, “Performance evaluation of a modified pyramid solar still

employing wick, reflectors, glass cooling and TiO2 nanomaterial," *Desalination*, V. 539, no. January, 2022, doi: 10.1016/j.desal.2022.115939.

[29] Z. S. Abdel-Rehim and A. Lasheen, "Experimental and theoretical study of a solar desalination system located in Cairo, Egypt," *Desalination*, V. 217, no. 1–3, pp. 52–64, Nov. 2007, doi: 10.1016/j.desal.2007.01.012.

[30] H. Amiri, M. Aminy, M. Lotfi, and B. Jafarbeglo, "Energy and exergy analysis of a new solar still composed of parabolic trough collector with built-in solar still," *Renew Energy*, V. 163, pp. 465–479, Jan. 2021, doi: 10.1016/j.renene.2020.09.007.

[31] M. Elashmawy, "An experimental investigation of a parabolic concentrator solar tracking system integrated with a tubular solar still," *Desalination*, V. 411, pp. 1–8, 2017, doi: 10.1016/j.desal.2017.02.003.

[32] M. Elashmawy, "Improving the performance of a parabolic concentrator solar tracking-tubular solar still (PCST-TSS) using gravel as a sensible heat storage material," *Desalination*, V. 473, Jan. 2020, doi: 10.1016/j.desal.2019.114182.

[33] M. Elashmawy, "Effect of surface cooling and tube thickness on the performance of a high temperature standalone tubular solar still," *Appl Therm Eng*, V. 156, pp. 276–286, Jun. 2019, doi: 10.1016/j.applthermaleng.2019.04.068.

[34] M. Elashmawy and F. Alshammari, "Atmospheric water harvesting from low humid regions using tubular solar still powered by a parabolic concentrator system," *J Clean Prod*, V. 256, May 2020, doi: 10.1016/j.jclepro.2020.120329.

[35] F. A. Essa, A.S. Abdullah, Wissam H. Alawee, A. Alarjani, Umar F. Alqsair, S. Shanmugan, Z.M. Omara, M.M. Younes, "Experimental enhancement of tubular solar still performance using rotating cylinder, nanoparticles' coating, parabolic solar concentrator, and phase change material," *Case Studies in Thermal Engineering*, V. 29, Jan. 2022, doi: 10.1016/j.csite.2021.101705.

[36] U. F. Alqsair, A. S. Abdullah, and Z. M. Omara, "Enhancement the productivity of drum solar still utilizing parabolic solar concentrator, phase change material and nanoparticles' coating," *J Energy Storage*, V. 55, Nov. 2022, doi: 10.1016/j.est.2022.105477.

[37] B. Chaouchi, A. Zrelli, and S. Gabsi, "Desalination of brackish water by means of a parabolic solar concentrator," *Desalination*, V. 217, no. 1–3, pp. 118–126, Nov. 2007, doi: 10.1016/j.desal.2007.02.009.

[38] G. O. Prado, L. G. M. Vieira, and J. J. R. Damasceno, "Solar dish concentrator for desalting water," *Solar Energy*, V. 136, pp. 659–667, Oct. 2016, doi: 10.1016/j.solener.2016.07.039.

[39] S. Gorjian, B. Ghobadian, T. Tavakkoli Hashjin, and A. Banakar, "Experimental performance evaluation of a stand-alone point-focus parabolic solar still," *Desalination*, V. 352, pp. 1–17, Nov. 2014, doi: 10.1016/j.desal.2014.08.005.

[40] Z. M. Omara and M. A. Eltawil, "Hybrid of solar dish concentrator, new boiler and simple solar collector for brackish water desalination," *Desalination*, V. 326, pp. 62–68, Oct. 2013, doi: 10.1016/j.desal.2013.07.019.

[41] M. Bahrami, V. Madadi Avargani, and M. Bonyadi, "Comprehensive experimental and theoretical study of a novel still coupled to a solar dish

concentrator," *Appl Therm Eng*, V. 151, pp. 77–89, Mar. 2019, doi: 10.1016/j.applthermaleng.2019.01.103.

[42] A. Abubakkar, P. Selvakumar, T. Rajagopal, and A. Tamilvanan, "Development of concentrating dish and solar still assembly for sea water desalination," in *Materials Today: Proceedings*, Elsevier Ltd, 2021, pp. 974–980. doi: 10.1016/j.matpr.2020.03.043.

[43] M. R. Al_qasaab, Q. A. Abed, and W. A. Abd Al-wahid, "Enhancement The Solar Distiller Water By Using Parabolic Dish Collector With Single Slope Solar Still," *Journal of Thermal Engineering*, V. 7, no. 4, pp. 1001–1015, May 2021, doi: 10.18186/thermal.931352.

[44] M. A. Tawfik, M. El-Tohamy, A. A. Metwally, A. M. Khallaf, and W. E. Abd Allah, "Experimental and numerical investigation of thermal performance of a new design solar parabolic dish desalination system," *Appl Therm Eng*, V. 214, Sep. 2022, doi: 10.1016/j.applthermaleng.2022.118827.

[45] K. Srithar, T. Rajaseenivasan, N. Karthik, M. Periyannan, and M. Gowtham, "Stand alone triple basin solar desalination system with cover cooling and parabolic dish concentrator," *Renew Energy*, V. 90, pp. 157–165, 2016, doi: 10.1016/j.renene.2015.12.063.

[46] T. Arunkumar, D. Denkenberger, R. Velraj, R. Sathyamurthy, H. Tanaka, and K. Vinothkumar, "Experimental study on a parabolic concentrator assisted solar desalting system," *Energy Convers Manag*, V. 105, pp. 665–674, 2015, doi: 10.1016/j.enconman.2015.08.021.

[47] W. B. Stine and R. B. Diver, "A compendium of solar dish/Stirling technology," 1994.

[48] Y. A. Cengel, A. J. Ghajar, and M. Kanoglu, “Heat and mass transfer: fundamentals and applications”.

[49] A. R. El-Shamy, R. Y. Sakr, N. S. Berbish, and M. H. Messra, “Experimental and Numerical Study of Forced Convection Heat Transfer From an Inclined Heated Plate Placed Beneath a Porous Medium,” *University Engineering Journal, JAUES*, V. 2, no. 4, 2007.

[50] R. S. Figliola and D. E. Beasley, “Theory and design for mechanical measurements,” *Meas Sci Technol*, V. 12, no. 10, p. 1743, 2001.

[51] A. S. Morris, “Measurement and Instrumentation Principles,” *Meas Sci Technol*, V. 12, no. 10, pp. 1743–1744, 2001, doi: 10.1088/0957-0233/12/10/702.

[52] S. J. Kline, “Describing uncertainties in single-sample experiments,” *Mech. Eng.*, V. 75, pp. 3–8, 1963.

[53] F. Stern, “Summary of Experimental Uncertainty Assesment Methodology with Example,” *IIHR Technical Report No. 406*, 1999.

[54] J. P. Holman, “Experimental Methods for Engineers Eighth Edition.” [Online]. Available: www.mhhe.com/holman

[55] M. M. Z. Ahmed, F. Alshammari, I. Alatawi, M. Alhadri, and M. Elashmawy, “A novel solar desalination system integrating inclined and tubular solar still with parabolic concentrator,” *Appl Therm Eng*, V. 213, Aug. 2022, doi: 10.1016/j.applthermaleng.2022.118665.

[56] L. Wang, X. Ma, Y. Zhao, R. Jin, and H. Zheng, “Performance study of a passive vertical multiple-effect diffusion solar still directly heated by parabolic

concentrator," *Renew Energy*, V. 182, pp. 855–866, 2022, doi: 10.1016/j.renene.2021.09.074.

[57] A. E. Kabeel, "Performance of solar still with a concave wick evaporation surface," *Energy*, V. 34, no. 10, pp. 1504–1509, 2009, doi: 10.1016/j.energy.2009.06.050.

[58] M. Jobrane, A. Kopmeier, A. Kahn, H. M. Cauchie, A. Kharroubi, and C. Penny, "Theoretical and experimental investigation on a novel design of wick type solar still for sustainable freshwater production," *Appl Therm Eng*, V. 200, no. September 2021, p. 117648, 2022, doi: 10.1016/j.applthermaleng.2021.117648.

[59] "Bottled water - prices by country, around the world, September 2022 | GlobalProductPrices.com." Accessed: Apr. 14, 2023. [Online]. Available: https://www.globalproductprices.com/rankings/mineral_water_prices/

[60] V. Velmurugan, C. K. Deenadayalan, H. Vinod, and K. Srithar, "Desalination of effluent using fin type solar still," *Energy*, V. 33, no. 11, pp. 1719–1727, 2008, doi: 10.1016/j.energy.2008.07.001.

[61] A. A. El-Sebaii and M. El-Naggar, "Year round performance and cost analysis of a finned single basin solar still," *Appl Therm Eng*, V. 110, pp. 787–794, 2017, doi: 10.1016/j.applthermaleng.2016.08.215.

[62] Z. Fayaz, G. S. Dhindsa, and G. S. Sokhal, "Experimental study of solar still having variable slope tilted wick in the basin to enhance its daily yield," in *Materials Today: Proceedings*, Elsevier Ltd, 2021, pp. 1421–1426. doi: 10.1016/j.matpr.2021.09.195.

Appendix A Thermocouple Calibration

All temperature sensors were calibrated in the laboratory against a mercury-in-glass thermometer, which has an accuracy of ± 0.5 ℃. A representation of the obtained calibration curves alongside the associated fitted equations is presented in Fig. A.1.

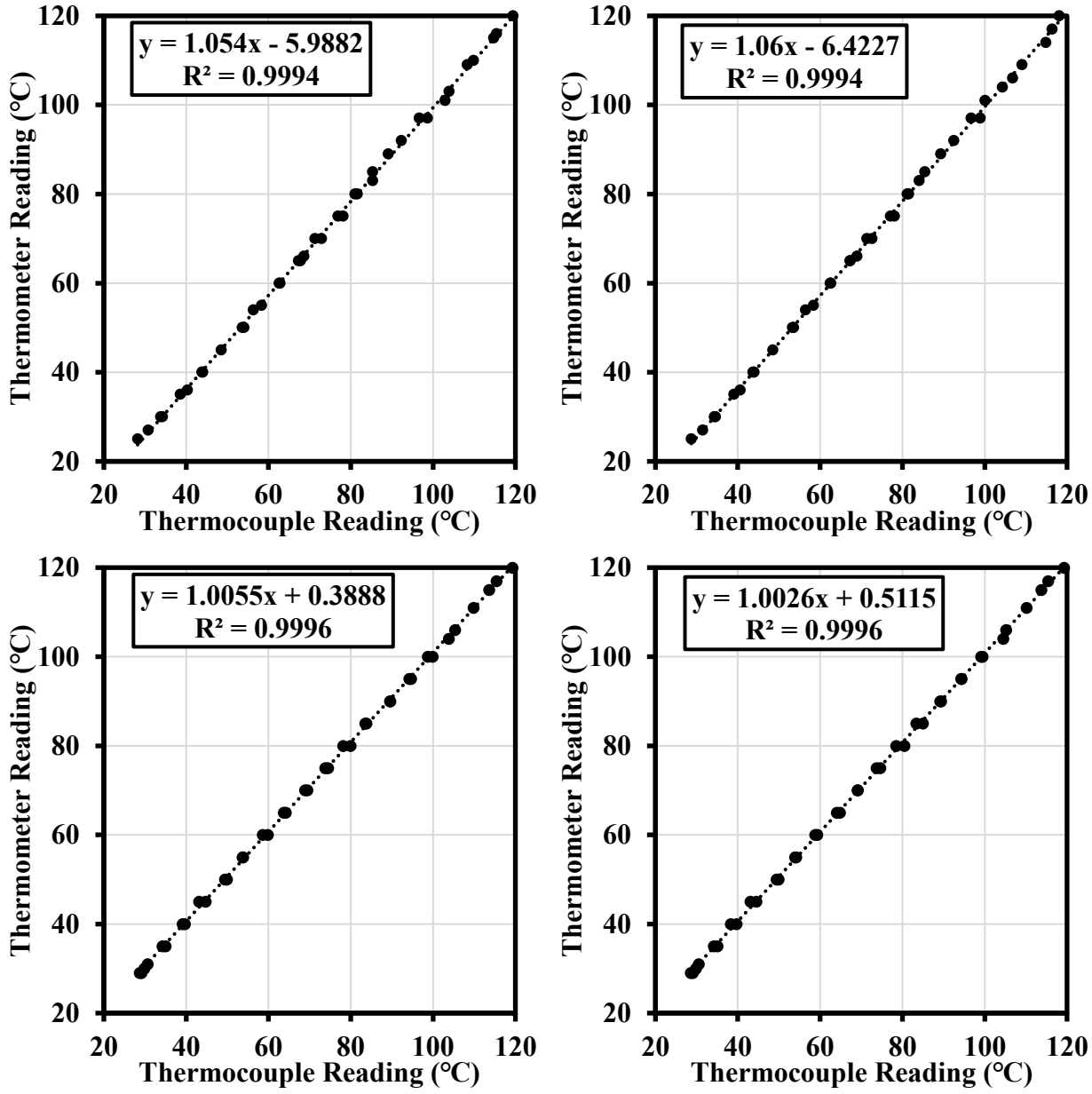

Fig. A.1 Thermocouple calibration curves.

Appendix B Uncertainty Analysis

This appendix presents a comprehensive assessment of the uncertainty associated with the solar desalination system parameters, which were determined in CHAPTER 4. This assessment relies on the measurement uncertainties inherent in the measurement devices utilized to collect experimental data. The uncertainty calculation method follows the root sum square combination, which effectively accounts for the cumulative effects of each input. This approach, as outlined by Kline, Stern, and Holman [50]-[52], ensures a careful examination of uncertainty, offering a strong framework for analysis and interpretation.

The maximum total uncertainty associated with the daily distilled productivity and daily system efficiency can be computed from the case depicted in Table B.1.

Table B.1 Uncertainties of main parameters within the case.

Parameter	**Uncertainty**
Density (ρ)	1 kg/L± 0 kg/L
Volume (V)	6.783 L ± 0.025 L
Latent heat of vaporization (h_{fg})	2257000 J/kg ± 0 J/kg
Area of dish (A)	1.131 m^2 ± 0 m^2
Time (t)	36000 s ± 0 s
DNI	876.92 W/m^2 ± 10 W/m^2

B.1 Uncertainty in The Daily Distilled Productivity

The daily distilled productivity is computed according to the Equation (B.1). Hence, the maximum uncertainty in the daily distilled productivity can be determined from Equation (B.2):

$$m = \rho \times V = 1 \times 6.783 = 6.783\ kg \tag{B.1}$$

$$\frac{\omega_m}{m} = \pm\sqrt{\left(\frac{1\times\omega_\rho}{\rho}\right)^2 + \left(\frac{1\times\omega_V}{V}\right)^2} = \pm\sqrt{\left(\frac{1\times0}{1}\right)^2 + \left(\frac{1\times0.025}{6.783}\right)^2} = \pm0.0037 = \pm0.37\% \quad \text{(B.2)}$$

B.2 Uncertainty in The Daily System Efficiency

The daily system efficiency can be determined by Equation (4.12). Consequently, the maximum uncertainty in the daily system efficiency can be obtained by Equation (B.3):

$$\frac{\omega_\eta}{\eta} = \pm\sqrt{\left(\frac{1\times\omega_m}{m}\right)^2 + \left(\frac{1\times\omega_{h_{fg}}}{h_{fg}}\right)^2 + \left(\frac{-1\times\omega_{DNI}}{DNI}\right)^2 + \left(\frac{-1\times\omega_A}{A}\right)^2 + \left(\frac{-1\times\omega_t}{t}\right)^2} = \pm\sqrt{\left(\frac{1\times0.025}{6.783}\right)^2 + \left(\frac{1\times0}{2257000}\right)^2 + \left(\frac{-1\times10}{876.92}\right)^2 + \left(\frac{-1\times0}{1.131}\right)^2 + \left(\frac{-1\times0}{36000}\right)^2} = \pm0.012 = \pm1.12\% \quad \text{(B.3)}$$

الملخص العربي

الندرة المائية تظل تحديا عالميا حرجاً، خصوصاً في المناطق القاحلة وشبه القاحلة حيث يكون الوصول إلى المياه العذبة محدوداً. لذلك يعتبر تطوير أساليب فعالة ومستدامة لإنتاج المياه العذبة أمراً أساسيا لضمان رفاهية المجتمعات والحفاظ على النظم البيئية. تقدم المقطرات الشمسية المركزة وسيلة واعدة لمواجهة هذا التحدي من خلال تسخير الطاقة الشمسية لإنتاج الماء المقطر من مصادر المياه المالحة أو قليلة الملوحة.

شهدت الدراسة الحالية تقييمًا تجريبيًا لمقطر شمسي مركز جديد لتتبع أشعة الشمس ضمن الظروف المناخية المصرية خلال صيف عام 2022. ويشتمل نظام المقطر الشمسي المقترح على مرآة عاكسة مكافئة قطرها 120 سم مزودة بآلية تتبع ثنائية المحور، مما يضمن التقاط الطاقة الشمسية بشكل مثالي. خلال اليوم. إلى جانب مقطر شمسي أسطواني يبلغ حجمه 3.7 لتراً مُثبت في نقطة التركيز، يحقق النظام نسبة تركيز تبلغ 12.5، مما يزيد من كفاءة عمليات تبخير وتكثيف الماء.

تم دراسة معاملين اثنين حاسمين في هذا البحث: ملوحة مياه التغذية ونسبة ملء المياه المالحة داخل المقطر الشمسي. من خلال تقييم ثلاث عينات من مياه التغذية بمستويات مختلفة من الملوحة (17، 27، و37 جزءاً في الألف) وأربع نسب مختلفة لملء المياه المالحة (26.5٪، 39.8٪، 53.1٪، و66.3٪)، تم التوصل إلى رؤى حول تأثير هذه العوامل على أداء النظام.

في حين أن زيادة ملوحة مياه التغذية أظهرت تأثيرًا ضئيلًا على إنتاجية المقطر الشمسي، فإن التغييرات في نسبة ملء المياه المالحة أدت إلى تأثيرات ملحوظة. لوحظ أن رفع نسبة الملء من 26.5٪ إلى 53.1٪ أدى إلى تحسين ملحوظ في كل من الإنتاجية التراكمية اليومية وكفاءة النظام بنسبة 22.69٪ و26.34٪ على التوالي. ومع ذلك، أدت الزيادة الإضافية في نسبة الملء إلى 66.3% إلى انخفاض في الإنتاجية التراكمية اليومية وكفاءة النظام بنسبة 7.06٪ و6.87٪ على التوالي. بالإضافة إلى ذلك، أدت زيادة ملوحة مياه التغذية من 17 جزء في الألف إلى 37 جزء في الألف إلى انخفاض الإنتاجية التراكمية اليومية بنسبة تقدر بحوالي 5.61% وكفاءة النظام اليومية بنسبة 5.1%.

تم تحديد الإنتاجية التراكمية اليومية للنظام لتكون 6 كجم/م2، عند نسبة ملء مثالية تبلغ 53.1٪، مما يحقق معدل كفاءة يومي للنظام يبلغ 42.88٪. بالإضافة إلى ذلك، تم تقدير متوسط التكلفة المرتبطة بإنتاج المياه العذبة بمقدار 0.0489 دولار/لتر. ومن الجدير بالذكر أن النظام المقترح حقق أعلى كفاءة لحظية بلغت 61.77% وأقصى معدل إنتاجية للمياه المقطرة بمقدار 0.941 كجم/ساعة.م^2.

جامعــة بنــها

كليــة الهندســة بشبرا

قســم الهندسة الميكانيكية

"دراسة و تحليل أداء مقطر شمسي مركز"

رسالة مقدمة إلى كلية الهندسة بشبرا، جامعة بنها كجزء من متطلبات الحصول على درجة ماجستير العلوم في الهندسة الميكانيكية (هندسة القوى الميكانيكية)

مُقدمة من

المهندس/ محمد محمود ضيف محمد

بكالوريوس هندسة القوى الميكانيكية
معيد بقسم الهندسة الميكانيكية
كلية الهندسة بشبرا ــ جامعة بنها

تحت إشــراف

أ. د/ أحمد عطية عبد اللطيف
قسم الهندسة الميكانيكية
كلية الهندسة بشبرا
جامعة بنها

أ. م. د/ محمد السيد محمد امام
قسم الهندسة الميكانيكية
كلية الهندسة بشبرا
جامعة بنها

د/ علي محمد أحمد سليمان
قسم الهندسة الميكانيكية
كلية الهندسة بشبرا
جامعة بنها

القاهرة – جمهورية مصـر العربيــة

2024